Master Thesis
TVVR 16/5011

Wave transformation at a rock platform in Victoria, Australia

A study combining field measurements with numerical modelling

Hanna Kowalczyk

Division of Water Resources Engineering
Department of Building and Environmental Technology
Lund University

Wave transformation at a rock platform in Victoria, Australia

A study combining field measurements with numerical modelling

By:
Hanna Kowalczyk

Master Thesis

Division of Water Resources Engineering
Department of Building & Environmental Technology
Lund University
Box 118
221 00 Lund, Sweden

Water Resources Engineering
TVVR-16/5011
ISSN 1101-9824

Lund 2016
www.tvrl.lth.se

Master Thesis
Division of Water Resources Engineering
Department of Building & Environmental Technology
Lund University

English title:	Wave transformation processes at a rock platform in Victoria, Australia – A study combining field measurements with numerical modelling
Author:	Hanna Kowalczyk
Supervisor:	Magnus Larson, David M. Kennedy
Examiner:	Hans Hanson
Language	English
Year:	2016
Keywords:	Wave dynamics, wave modelling, shore platform, rock coasts, EBED

Abstract

Even though a large part of the world's coastline consists of rocky shores, it is still a neglected field of study in coastal research. To increase the knowledge of wave transformation processes on these shores is important in order to understand erosional patterns and to manage coastal risks. In this study, the wave transformation processes on and off a rock platform in Victoria, Australia, have been described and analyzed through a combination of mathematical modelling and field measurements. The results show that the chosen field site possesses rather unique and complex conditions for wave transformation. Waves with extremely large angles in combination with a complicated bathymetry in the nearby surroundings, and a deviation from the standard shape of the wave spectrum, creates a difficult situation for wave modelling. The chosen model has not been able to accurately reproduce the trends seen in the data but has highlighted the importance of the nearshore bathymetry and the offshore wave conditions as controlling factors on the characteristics of the waves reaching and propagating onto rock platforms.

Keywords: Wave dynamics, wave modelling, shore platform, rock coasts, EBED

Contents

1 Introduction

1.1 Background

A large part of the world's coastline consists of rocky shores. It is however difficult to confidently quantify exactly how big this part is. In the same way it is difficult to estimate the global coverage of rocky shore platforms. This is mainly due to the fact that the definition of a rocky shore is not completely clear and there is no global categorization scheme for landforms within the larger term 'rocky shores'. Visual data analysis and well defined terminology could in the future help with this issue [Naylor et al., 2010]. An estimation performed by Short and Woodroffe [2009] suggests that as much as 40 percent of the Australian coast line consists of rocky shores. Despite this large quantity of rocky shores, they have been a neglected field of study compared to other coasts such as beaches or salt marches [Naylor et al., 2010] [Stephenson, 2000] [Trenhaile, 2002]. Naylor et al. [2010] performed an investigation of the representation of rocky shores in coastal research and found an underrepresentation both in scientific papers and in textbooks. The neglect of this coastal landform can mostly be explained by the greater interest in other landforms, such as beaches and wetlands, which historically have had a greater interaction with and been of greater economic importance to humans. Such rapidly changing landforms have also been considered as more vulnerable to sea level rise and thus been the focus of climate change related coastal research [Trenhaile, 2002]. There are many arguments for why more rocky shore related research should be done and why wave dynamics at these shores are important. The three most prominent motivations identified in this report are (1) coastal erosion, (2) coastal hazards and (3) vulnerability to climate change. Below follows a short description of the main concepts regarding these three motivations.

Rocky shores are an erosional landform controlled by both subaerial and marine processes. There has been some discussion among researchers, if there is a dominant factor and how and if the two processes work together [e.g. Ogawa et al., 2011, Naylor et al., 2010]. It is therefore not clear how and when rocky shores are formed and what processes occur on this type of coast. The recreational usage of rocky shores and the development in their nearby area, is increasing [Thom, 2004]. It is therefore important to understand the erosional processes on this type of shore, in order to apply the right management strategies of such sites. Rocky shores are also believed to be important as a sediment source for other landforms and it is important to understand this connection in order to draw correct conclusions about overall erosion and deposition processes on the coastline [Trenhaile, 2002]. Wave induced erosion has been identified as an important factor for morphological change on rocky coasts and it is therefore important to understand the wave dynamics on and off the landform [Ogawa et al., 2011]

Figure 1: A rocky Victorian coastline lined with rock platforms. The studied field site is located at the second bay in the picture.

[Stephenson, 2000].

When people use rocky shores, and rock platforms in particular, for recreational purposes it entails a risk of people getting injured or killed on such coasts. In fact drowning accidents are already fairly common. The main hazard people face on rock platforms are waves. There have been several incidents where rock fishermen have been swept out to see by the swash from waves. It is therefore important to understand the wave dynamics at these type of shores in order to apply risk minimizing strategies. [Kennedy et al., 2013] [Tsai et al., 2004] [Shand et al., 2009]

Climate change has been seen as not very relevant for slow response landforms such as rocky shores. This slow response might however be more a weakness than an advantage. More dynamic systems have a chance to adjust to sea level rise whereas rocky platforms might be lost below the surface. An important source of sediment and ecosystem might be lost. Wave driven processes on these shores are important in order to understand the factors that drive platform evolution and hence the response to sea level rise.[Naylor et al., 2010]

1.2 Objectives

Limited research has been done on wave dynamics and wave transformation processes on rocky shore platforms. Increasing the understanding of wave dynamics at such features is important both when looking at erosional patterns of the landform and when analyzing risks and hazards on rocky shores. Numerical nearshore models have previously been a powerful tool to describe and understand wave processes in coastal areas but have traditionally been developed for, and validated on, mildly sloping sandy beach profiles. The applicability of these models on other coastal landforms, such as coral reefs and rocky coasts, with sometimes very steep, almost vertical, slopes and complex morphology is not jet clear. The fact that the parameterizations of wave breaking, bed stress and other processes are derived from beach environments is another concern [Buckley et al., 2014].

The main objective of the thesis work is to analyze and describe the wave transformation processes on and off a rocky shore platform, through a combination of mathematical modeling and field measurements. The measurements were performed at a coastal location in Victoria, Australia. The data collected was firstly analysed to give a general understanding of the wave transformation processes in the area, and secondly used to investigate the applicability of a two-dimensional numerical model of nearshore waves on this type of coast.

1.3 Procedure

A literature review of wave dynamics in shallow waters in addition to related studies on rocky shore platforms was carried out. From the literature, important theory, concepts, conclusions and available suitable data was collected for comparison and analysis.

Field measurements were performed offshore from, and on a microtidal rocky shore platform in Victoria, Australia. A transect of four pressure sensors was deployed across the platform in addition to a transect of five sensors stretching from close to the edge of the platform and 1.5 km offshore. The raw data was analyzed statistically according to methods used in similar research studies. The results were then compared and analyzed with respect to the results obtained from the literature review and the wave characteristics and transformation processes found in the data were identified.

The recorded offshore waves were used as input for wave model simulations by a multi-directional random wave transformation model (EBED) formulated by Mase [2001] and modified by Nam et al. [2009]. Four main model runs, with differing input data, were performed and compared to the field data in order to investigate the applicability of the model and identify its deficiencies and strengths. The results were then analyzed to describe the underlying wave transformation processes present at the site.

1.4 Outline

This report will firstly introduce some of the most important concepts and parameters used to describe and explain wave characteristics, processes and wave transformation in the nearshore area. The result of the literature review is then presented, containing an introduction to rock platform terminology as well as important findings from previous studies on the topic of wave transformation on rock platforms. The report will then focus on describing the methodology of the field measurements and model simulations before presenting and analyzing the results. The results will then be discussed and concluded.

2 Wave Theory

For centuries scientists, mathematicians and engineers have tried to describe and explain the motion of ocean water waves. One of the most fundamental wave theories is the so called linear wave theory, or Airy wave theory after its founder George Airy, which has been the basic theory for surface ocean waves for about 150 years [Holthuijsen, 2007]. Since then many theories and models have been developed with the goal to describe the complexness that is ocean waves. These theories and models are usually based on a combination of theoretical and empirical concepts. This chapter aims to describe the most important concepts, parameters and processes related to wave conditions in deep water and the transformation of waves as they move towards the shore into shallower water.

Several parameters are important for describing waves. The most important parameters used in this report are briefly described below and shown in Figure 2. [CEM, 2002]

- Wave height, H, defined as the distance between the wave *crest*, the highest point of the wave, and the *trough*, the lowest point of the wave.
- Wavelength, L, defined as the horizontal distance between two identical points on successive waves, e.g. the distance between two crests or two troughs.
- Wave period, T, defined as the time between the passage of two successive crests, or troughs, of a specific point.
- Wave frequency, f, related to wave period according to $f = 1/T$.
- Phase velocity or wave celerity, C, the speed of propagation, where $C = L/T$

2.1 Describing ocean waves

It is simple to derive the desired wave parameters and comparably easy to describe a wave climate and it's processes when looking at a wave field of regular or monochromatic waves, i.e. waves with a constant period and height. When looking at the irregular surface of the ocean and the randomness of a natural wave climate, this is not as trivial and statistical methods are needed to describe the wave field CEM, 2002. In this section firstly some of the different type of waves are presented followed by an explanation of the two main methods used to interpret and describe natural wave conditions.

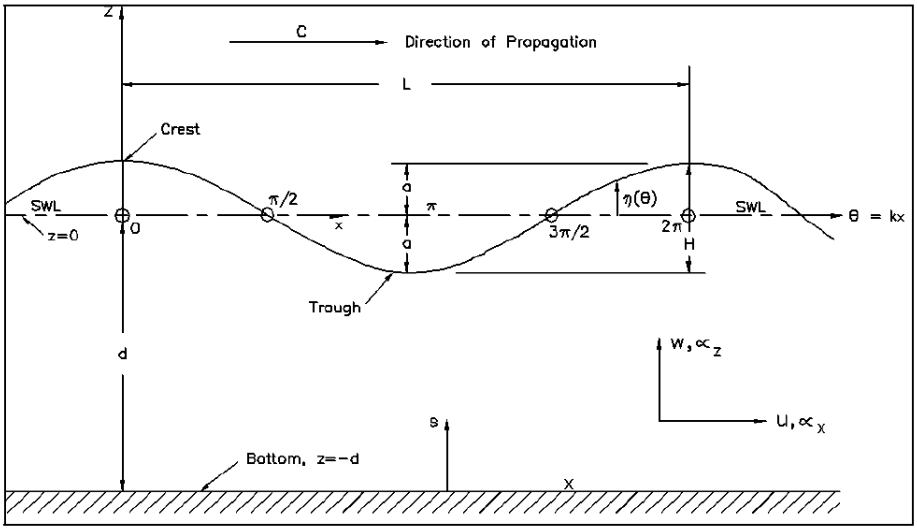

Figure 2: Illustration of wave parameters [CEM, 2002]

2.1.1 Wave types

There are many different ways to describe and classify waves. One common way is categorization depending on the process creating the wave, where waves of different origin can be described in terms of their period, T, or frequency,f (where $T = 1/f$). The different types of waves and their corresponding period/frequency is shown in Figure 3.

Generally when we talk about waves found on the ocean surface, we mean wind generated gravity-waves (GW). These waves are formed by the shear stress between the water surface and the wind, where the force of gravity is striving to restore equilibrium. Such waves generally have a period of 3-25 s and are an important force in the coastal regions of the world [CEM, 2002]. Surface wind waves are usually divided into two types: *seas* and *swells*. Waves that are generated and still affected by the wind are called seas, but when the waves have moved out of their generating area they are instead referred to as swell. Swell contains waves of more regular nature with longer periods and well-defined long crests. Seas are irregular, more chaotic and characteristically have a shorter period and length [CEM, 2002]. The creation of swell can be explained by the fact that waves propagate with different speed depending on their wave length. During a storm, sea is created, containing a spread of waves with wave periods between 3-25 s. A longer period wave travels faster than a shorter wave. In

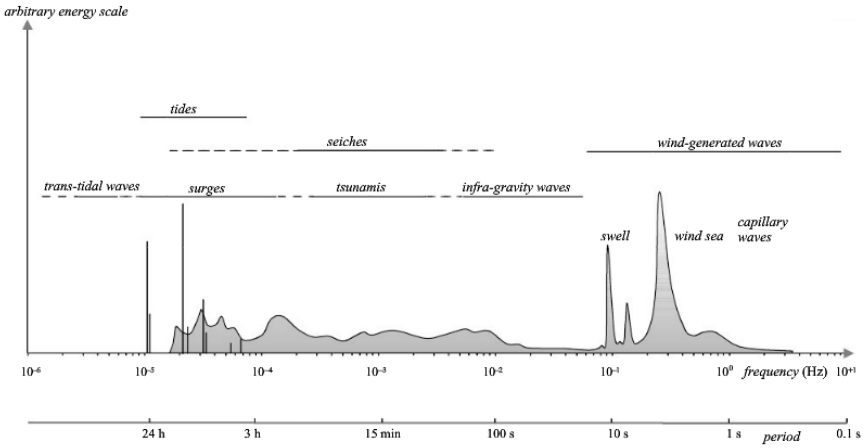

Figure 3: Frequencies and periods for different types of waves (after Munk [1950], figure from [Holthuijsen, 2007]

addition wave energy is transferred from short period waves to waves with a longer period. This results in a type of sorting of waves, leading to long period waves, swell, moving away from the area of wave generation CEM, 2002. These type of waves are typically what reaches a coastal area and thus important for shaping and creating near shore environments. Very short wind-generated waves are called capillary waves, and here, surface tension is the the main force striving for equilibrium [Holthuijsen, 2007].

Infragravity waves (IGW) have longer periods, typically a few minutes, and are formed by the nonlinear interaction of the shorter gravity waves. Such interactions are most common in the nearshore area where the energy of shorter waves varies rapidly. One of the forms of infragravity waves are formed due to the fact that waves tend to reach the coast in groups. The water surface then oscillates almost periodically with the wave groups, causing wave set-up to move periodically as well. This causes the surf zone to move up and down, with the period of the wave groups, causing waves, with a frequency in the infragravity band, to move out to sea.[Holthuijsen, 2007]

Other waves, with longer periods, such as tides, tsunamis and storm surges exist but are not the focus of this report and hence will not be described in detail.

2.1.2 Wave-by-wave approach

When analyzing natural wave climates it is common to investigate the time-varying change of the sea surface elevation in one point. From this record individual waves are then identified and represented by a height and period. This is called the wave by wave approach. There are a few different methods for identifying waves, here, the zero-down crossing method is explained. When using this method a wave is defined as being the profile of the water surface elevation between two successive mean water level downward crossings of the surface. A zero-down crossing is when the water level goes from being above the mean water level, or zero, to being below the mean. This means a wave starts just when the surface elevation has crossed the mean water level in a downward direction, the surface elevation will then continue to decrease to a minimum before increasing again until it crosses zero in an upward direction. The surface elevation will then increase until it reaches a maximum and decrease again until it crosses the mean water level in a downward direction. This is the end of the wave. The wave height is defined as the distance between the minimum and maximum surface elevation in a wave. The wave period is defined as the time between two zero-down crossings.This concept is illustrated in Figure 4. [Holthuijsen, 2007][CEM, 2002]

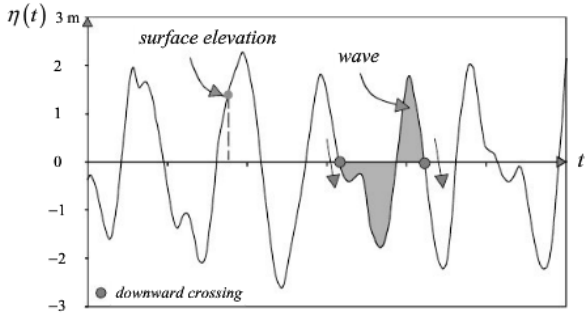

Figure 4: Illustration of the definition of a wave in a time series of surface elevation by the zero-down crossing method. [Holthuijsen, 2007]

2.1.3 The wave spectrum

One of the most commonly used tools when analyzing waves and wave records is the wave spectrum. Simplified, this is a way of describing the distribution of waves over different frequencies for a specific sea condition. To do this it is assumed that a snapshot of the sea surface, or a record of the fluctuations of a

specific point at the sea surface over time $\eta(t)$, is one observation of an underlying statistic process which can be obtained using mathematical tools. This is done by using the concept of Fourier series, which states that almost any function can be described by the summation of a large or infinite amount of harmonic wave components. This means that the sea surface $\eta(t)$ can be described according to Equation 1:

$$\eta(t) = \sum_{i=1}^{N} a_i cos(2\pi f_i t + \alpha_i) \tag{1}$$

where a_i and α_i are the amplitude and phase of each discrete frequency $f_i = i/D$ $(i = 1, 2, 3, ...)$, where D is the duration of the wave record. This means that we would get an amplitude and a phase for each frequency and we can hence build an amplitude and a phase spectrum which represents the wave record (see Figure 5 and 6).

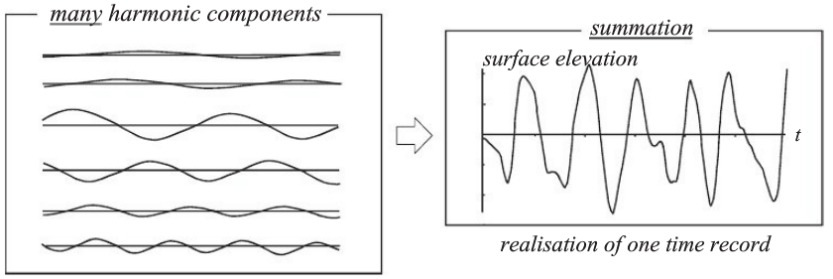

Figure 5: The summation of many different harmonics with constant, randomly chosen amplitudes and phases, creates one realization of the sea surface. [Holthuijsen, 2007]

For most wave conditions, especially for deep water waves, the phases are evenly distributed with no trend and the phase spectrum is therefore usually ignored. When looking at waves, the variance, defined as shown in Equation 2, is more useful, as it is related to wave height as well as wave energy. [Holthuijsen, 2007]

$$variance = \overline{\eta^2} = E\{\eta^2\} = \sum_{i=1}^{N} E\{\frac{1}{2}a_i^2\} \tag{2}$$

where $E\{\eta^2\}$ and $E\{\frac{1}{2}a_i^2\}$ are the expected values of η^2 and $\frac{1}{2}a_i^2$ respectively.

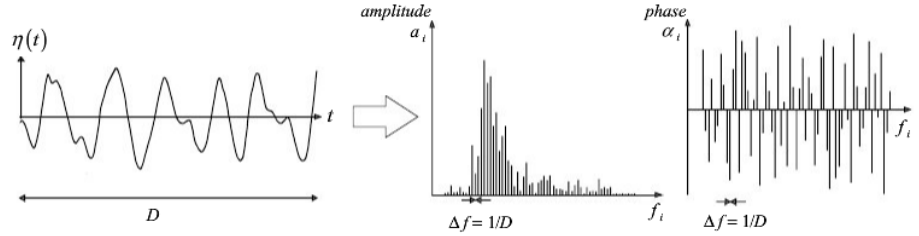

Figure 6: The amplitude and phase spectrum for one observation of the surface elevation. [Holthuijsen, 2007]

When taking a snapshot of the sea surface and analysing it, this is only one representation of the stochastic process. If we would take a snapshot a few seconds later the underlying process would still be the same, but the surface, and hence the variance spectrum, would look different. If we take an infinite amount of snapshots of the stationary stochastic process, the average of the variance spectrum would converge to one specific value for each frequency and we would have successfully represented the underlying process. This is difficult for real situations where the ocean is constantly changing. Luckily the changes are rather slow and we can confidently assume that the processes behind the sea surface elevation are stationary in a time period of around 15-30 min. There are different techniques to analyse such a rather short time series in order to obtain the underlying process. In this report a method called Welch's averaged modified periodogram method of spectral estimation is used. Simplified the method firstly divides the measured sequence into smaller, possibly overlapping, segments. These segments are then multiplied by a so called window function, in this report a Hamming's window is used. A window function is used to minimize the effects of so called spectral leakage which can occur when applying the Fourier transform on a sequence containing harmonics which are cut off. This naturally happens at the ends of a time series or smaller segments. When harmonics are cut off, the Fourier transform will not accurately pick up only the harmonics present. It will create artifacts in the spectrum, so called spectral leakage, and can produce a smearing around the actual frequency peaks. The Hamming's window decreases the intensity of the signal at the ends and hence this effect is minimized. The modified segments are then transformed using fast Fourier transformation creating so called modified periodograms. The final spectral analysis is the average of these periodograms. [Holthuijsen, 2007]

Another issue with deriving a wave spectrum from a measured time series is the fact that the series is not continuous. The series is made of discrete samples taken with a certain frequency, usually around one sample every 0.5 s i.e. a sample

rate of 2 Hz. Unfortunately this means that the analysis cannot pick up harmonics with very high frequencies, as these fall between the sampling points and cannot be distinguished by Fourier transform. This can cause an untrue amplification of some frequencies. Fortunately, this phenomena usually does not affect an ocean wave spectra as there are few waves with high frequencies present. In addition a high frequency cut-off is often added, where high frequency harmonics, not commonly present or of interest when looking at ocean waves, simply are cut out of the data. This also decreases the effect of high frequency noise in the measurements. [Holthuijsen, 2007]

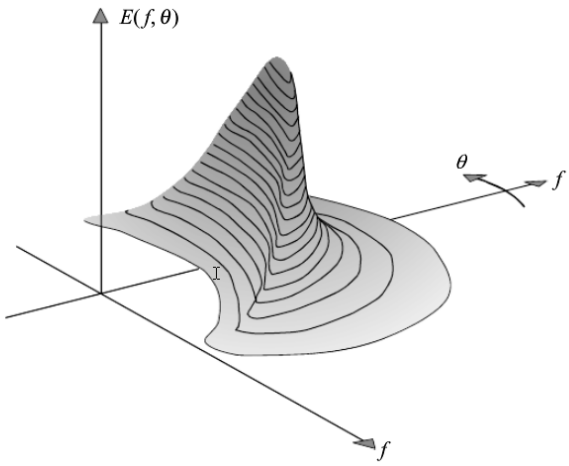

Figure 7: The two-dimensional frequency-direction spectrum of wind generated waves. [Holthuijsen, 2007]

The produced variance wave spectrum, or energy wave spectrum, gives a representation of the periodicity, i.e. the frequency, of the harmonics/the waves, in the wave record. It also gives an idea of at what frequencies most of the wave energy is located. It simply shows us if there are long period waves, or short period waves present, and how energetic these are. This can be very useful. By analysing the wave spectrum the wave climate can be described, this due to the fact that waves with different origin show specific characteristics. During a storm event, for example, a strong central peak with a fairly predictable shape can be seen. When the waves have moved a long distance away from the storm event, as swell, a single sharp peak can instead be seen. In shallow waters, when wave breaking is present, a pattern of one sharp peak with smaller peaks at harmonic frequencies can be seen. This pattern is due to the fact that waves at breaking are

highly nonsinusoidal and have a sharp crest and flat trough. Another conclusion which can be drawn from a wave spectrum is if there are infragravity waves, i.e. low frequency waves, present. By looking at a wave spectrum one or several of these patterns can be detected and will therefore give information about the origin and composition of the wave climate. [Holthuijsen, 2007]

The wave spectrum discussed in the above section, only describes the surface elevation in one point over time and does not describe the three-dimensional surface of the ocean. In order to describe the actual surface of the ocean the random-phase/amplitude model can be expanded by looking at a large sum of statistically indepentent harmonic waves propagating in x,y-space with a direction θ. This two-dimensional wave spectrum shows the distribution of the variance not only over the different frequencies but also over all directions, it is called the frequency-direction spectrum. By integrating the two-dimensional spectrum over all directions, the one-dimensional spectrum can be obtained. See Figure 7 for an example of a two-dimensional frequency-direction spectrum. [Holthuijsen, 2007]

2.1.4 Wave parameterization

Regardless what approach is chosen to analyse a wave field, wave by wave or wave spectrum, the same wave parameters are then generally derived and used for further analysis. Two of the most useful parameters when looking at waves is a characteristic wave height and period. These parameters are the product of trying to represent an irregular, natural wave field with simple parameters representing the characteristics of the wave field. There are several different parameters that can describe the statistics of an irregular wave field. One which is widely accepted, and mostly generates a reasonable and often conservative approximation, is the significant wave height. One can describe it as representing the wave field with one characteristic regular wave. This regular wave can then be used to describe the characteristic processes of the wave field. This concept is based on the fact that the wave conditions can be represented by a single wave. If the wave field has a great variation in wave period or direction this might not be an acceptable approximation and a different approach should be used [CEM, 2002]. The significant wave is defined as the mean of the highest one-third of waves in the wave record. The significant wave height and period for a wave record with N waves can then be determined both from zero-down crossing and a wave spectrum according to Equations 3 - 6. It should be noted that these two derivations do not always lead to the exact same value for the wave parameters, in fact, the spectral significant wave height, H_{m0}, tends to be around 5-10 % larger than the from time series estimated wave height, H_s. [Holthuijsen, 2007]

From zero-down crossing analysis:

$$significant\ wave\ height = H_s = \frac{1}{N/3}\sum_{i=1}^{N/3} H_i \tag{3}$$

$$significant\ wave\ period = T_s = \frac{1}{N/3}\sum_{i=1}^{N/3} T_i \tag{4}$$

where i is the rank number of the wave, based on wave height, i.e. $i = 1$ is the highest wave, $i=2$ is the second highest wave etc.. [Holthuijsen, 2007]

From wave spectrum:

$$significant\ wave\ height = H_{m0} = 4.0\sqrt{m_0} \tag{5}$$

$$significant\ wave\ period = T_s = 0.95T_p \tag{6}$$

where m_0 is the zeroth moment of the variance spectrum and T_p is the peak period defined as the inverse of the frequency at the main peak of the wave spectrum.[Holthuijsen, 2007]

Other commonly used parameters for parameterization are the mean wave height $\overline{H}$, the root-mean-square wave height H_{rms} and the maximum wave height H_{max} as well as the mean zero-crossing wave period $\overline{T_0}$ or the peak wave period T_p.

2.2 Nearshore processes

Shallow water waves are quite different from, and more complex than, deep water waves. When the waves propagate towards the shore into shallower water they eventually reach a point where the wave induced motion of water particles will be effected by the bottom. Some physical aspects of the wave are then changed. In this section the principles behind the, for this report, most relevant nearshore processes are explained.

2.2.1 Wave transformation processes

The three processes; refraction, diffraction and shoaling are so called propagation processes [CEM, 2002]. When waves move into shallower water and start interacting with the bottom, the bathymetry as well as shallow water structures will cause the waves to change direction and to convergence or divergence, leading to the concentration or spreading out of wave energy. This is due to the fact that the

velocity field of deep water wave motion extends to a depth equal to L/2 m into the water column. This means that if the water depth is less than L/2 m, then the wave motion interacts with the substrate and some of the physical aspects of the wave are changed. When waves start interacting with the bottom, most importantly, the wavelength, celerity and group velocity is affected. The consequences can be a change in direction (refraction) and in amplitude (shoaling) of the wave. The bathymetry of the near shore area is therefore very important for wave transformation. [CEM, 2002]

The effect of refraction can be explained by imagining a monochromatic wave propagating across a shallow water area with an even slope which is parallel to the shoreline, i.e. the water depth is decreasing in a constant rate when moving landward. If a wave propagates towards the shore on an angle, there will be a part of the wave that reaches shallow water conditions earlier than the remaining part of the wave crest. Wave speed decreases in shallow water, leading to that the shallower part of the wave will slow down, while the rest of the wave propagates with the same speed, causing the wave crest to change direction. This effect is called refraction and leads to waves changing their direction towards propagating closer to perpendicular to the shoreline or parallel to the bottom gradient. [CEM, 2002]

If assuming steady state and monochromatic waves, it follows that energy is conserved and wave period is constant. When the waves move into shallower water they slow down and wave length decreases. This means that the energy which is released due to decrease in wave celerity instead increases the wave height. This phenomena is called shoaling.[Holthuijsen, 2007].

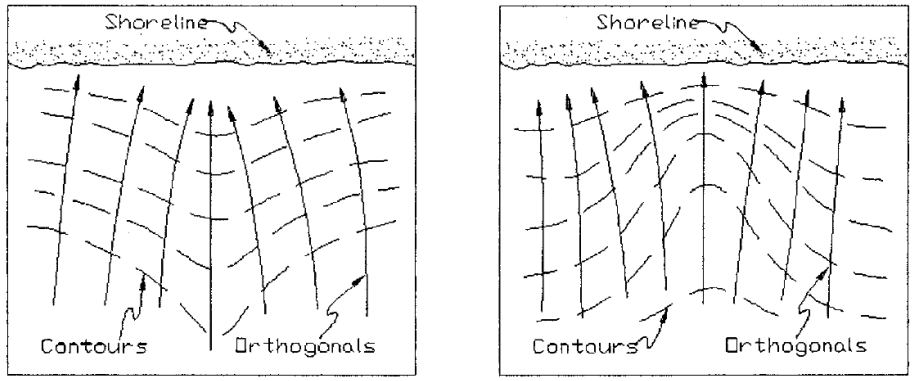

Figure 8: The change in energy patterns due to wave transformation processes. Focusing of energy due to a shoal on the left and spreading of energy due to a canyon on the left.[CEM, 2002]

Refraction and shoaling processes generally lead to a spread of total energy. If the waves are refracted across a simple parallel depth contour profile, a general decrease in energy can be seen when moving landward. If the bathymetry is more complex, different energy patters can be found. Shoals tend to spread out energy at the sides and focus waves onto the shoal, whereas canyons focus energy on the sides and reduce energy above the canyon (see Figure 8. [CEM, 2002])

When moving away from monochromatic waves and into irregular wave territory it is a lot more difficult to describe and predict refraction and shoaling. The processes might affect waves at each frequency differently, which can lead to a change in peak period of the wave field.[CEM, 2002]

The third propagation process is diffraction, which occurs if there is a large difference in wave amplitude between two connected areas. Such situations can occur if the wave crests encounter a sudden obstacle like a headland or breakwater. To demonstrate the effect of diffraction, imagine waves propagating in water of constant depth, perpendicular to an obstacle. Without diffraction the part of the wave crest hitting the obstacle would stop, while the remaining part of the wave crest would continue past the obstacle, without changing direction. This would mean that the obstacle would have a complete shadowing effect on the area behind it, and there would be no waves there. This is not the case. Instead, diffraction causes the wave energy to move from an area with higher wave heights to an area with lower wave heights. Due to this spreading of energy, the wave height in the incipient waves decrease during the diffraction process [CEM, 2002].

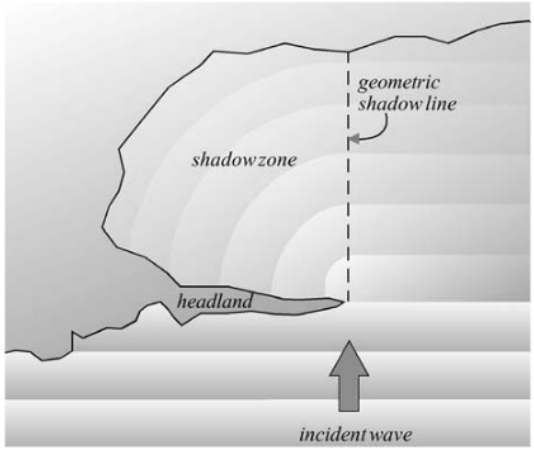

Figure 9: Diffraction pattern around a headland for a constant depth situation. [Holthuijsen, 2007]

2.2.2 Wave energy dissipation processes

In the nearshore area, waves not only change their shape and propagation characteristics, they can also lose energy. There are two main ways for wave energy dissipation to occur: (1) interaction with the bottom substrate through friction and percolation (flow into and out of the bed) and (2) wave breaking. The effect due to bottom-material, causing friction and percolation, is mostly ignored due to the difficulty of getting adequate information about the bottom- material composition[CEM, 2002]. In addition, these effects are generally only important over long distances [Holthuijsen, 2007].

The height of a gravity wave is physically limited. Stokes [2009] theoretically described that a wave will break when the velocity of the crest is greater than the propagation speed of the wave. This occurs at a certain wave steepness, H/L. Meaning that, for a wave with a certain length, there is a maximum wave height where the wave is so steep that it is no longer stable and will collapse. In deep water the wave height is limited by wave length. When moving into shallow water, the base of the wave is slowed down due to interaction with the bottom, whereas the crest is not as largely affected, causing the wave to break. Wave height is now also limited by water depth. [CEM, 2002]

The limiting wave steepness is different for deep and shallow wave conditions. For deep sea conditions it has been shown that the simple relationship of $H_0/L_0 = 0.141$ is satisfactory. In shallow areas the limiting wave steepness is instead expressed to be a function of relative water depth d/L and slope β. Many studies have tried to develop a relationship to predict the incident breaker height H_b. This is commonly done by trying to determine the nondimensional breaker index γ_b. Both the significant wave height, H_{m0}, the root-mean-square wave height, H_{rms} as well as the maximum wave height, H_{max} have been used for such analysis. It is therefore important to note which wave height is used before comparing values from different studies. The following terminology is used in this report:

$$\gamma_{b_{rms}} = H_{rms}/h \tag{7a}$$

$$\gamma_{b_{m0}} = H_{m0}/h \tag{7b}$$

$$\gamma_{b_{max}} = H_{max}/h. \tag{7c}$$

where h is water depth.

The most commonly used first estimate for breaker index is $\gamma_{b_{max}} = 0.78$. This relationship is between the maximum wave height, H_{max}, and water depth and was theoretically determined by McCowan [1891] for an isolated solitary wave on a horizontal surface. When looking at irregular waves it is common to instead

use eitherH_{m0} or H_{rms} to express the breaker index. When using this paremeters it should be noted that they are a representation of all waves present and do not differentiate between breaking and non breaking waves. The general first estimate breaker index, based on Thornton and Guza [1982], is then instead: $\gamma_{b_rms} = 0.45$ which can be converted to $\gamma_{b_{m0}} \approx 0.6$. Many other studies have been done on this topic, and have tried to describe the breaker index considering factors such as bottom friction, slope, currents, dispersion rate, level of nonlinearity etc. The breaker index is also often expressed as a truly empirical value, derived from field data and is commonly used in models used on near shore wave dynamics [Farrell et al., 2009].

3 Wave Dynamics on Rock Platforms

As mentioned previously there has been limited research on rocky shore platforms, including the wave dynamics on these type of coastal features. This section aims to briefly summarize and present relevant findings from previous studies on rock platforms.

When researching waves on rocky shore platforms some reoccurring parameters and relationships can be found. Most studies record the change of wave height and wave period across the platform over several tidal cycles. The data is then often analyzed by looking at:

1. The wave breaking index $\gamma_b = H/h$.
2. Wave energy attenuation.
3. The wave spectrum.

This section explains the terminology used, general conclusions made from previous studies, and more detailed descriptions of the three relationships mentioned above.

3.1 Terminology

Rocky platforms are divided into either Type A or type B. This categorization stems from the important book by Sunamura [1992]. A Type A platform is sloping seawards in a clear and uniform way, whereas Type B platforms are characterized by a distinctive seaward edge (see Figure 10). Field studies have shown that platforms with a greater slope, Type A, are more often occurring on coasts with a larger tidal range, macrotidal coasts, and Type B platforms are more common on microtidal coasts.[Trenhaile, 1987]

The characteristics between shore platforms, even within the same type, varies greatly. The features most important for wave dynamics are:

- ***The seaward edge*** - There has so far not been a uniform way of defining this feature. Definitions based on tides, biology, processes, morphology and sediment coverage have been used, leading to difficulties when comparing studies [Kennedy, 2015]. In this report the definition of the seaward edge will be as recommended by Kennedy [2015] in his review of the definitions of the seaward edge: *'The seaward edge is the point where active erosion of the bedrock ceases, characterized by erosional features such as notches and block-plucking scars or the deposition of sediment of such a thickness that the underlying bedrock is not exposed during storm events.'*.

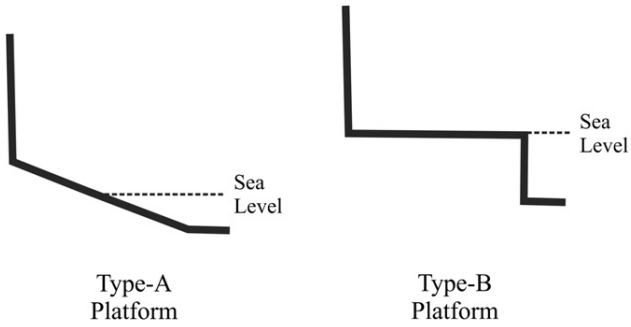

Figure 10: Typical shape of Type A and Type B platforms [Kennedy, 2015]

- ***The landward edge*** - It is common that the end of the platform, the landward edge, is easily identified due to a backing cliff. In other cases a beach or bigger boulders can cover the edge of the platform. For a sediment free platform, the landward edge is defined as the point where there is a clear change in angle away from the mean angle of the hinterland geology. If covered by sediment the landward edge is defined as the point where the total sediment column no longer is mobilized during decadal storm events.[Kennedy, 2015]
- ***Platform width*** - The distance between the seaward and landward edge of the platform.
- ***Platform gradient*** - The mean slope of the whole platform.
- ***Water depth on platform*** - The water depth on the platform is an important control for wave energy and will vary depending on tidal fluctuations as well as position on the platform. To consider the total range of water depths found on the platform it is common to observe the water depth on the platform for the mean sea level (MSL) the mean high spring tide (MHST) and the mean low neap tide (MLST).
- ***Water depth in front of platform*** - The water depth in front of the seaward edge is an important control for wave energy propagating onto the platform and will vary depending on the tide. Consistent with water depth on the platform, it is common to observe the water depth at MSL, MHST and MLST.
- ***Tidal fluctuations*** - The tide and its range determines the water level on and in front of the platform and is hence important. To describe the

tidal range it is common to observe only the spring tides, i.e. the highest tides. The mean spring tidal range is defined as the distance between the mean high water spring (MHWS) and the mean low water spring (MLWS). Where MHWS is the average of two successive high waters during spring tides over a year and MLWS is the average water height for two successive low waters during the same period [Simm et al., 1996].

3.2 General findings

When looking at wave dynamics on a rocky shore, previous research has generally been done from a geomorphological view point. The studies have identified key factors influencing the way the waves change their behaviour and their characteristics when propagating towards, onto and across a rocky shore platform. Few studies have though tried to quantify and explain these processes by using or comparing to numerical solutions or models.

The most general conclusion from previous research is that the morphology of the near shore area and the platform, together with tidal fluctuations, are important controls for wave dynamics on rock platforms [Stephenson and Kirk, 2000] [Ogawa et al., 2012] [Marshall and Stephenson, 2011] [Trenhaile and Kanyaya, 2007]. This simply means that, generally, the deep water waves move into an area, where the water is shallow enough to allow the waves to interact with the substrate, already before they reach the platform. The nature of this interaction is determined by the water depth and shape of the bottom. As mentioned in the previous section about shallow water waves, the waves are affected by the bathymetry of the bottom as well as the water depth, leading to processes such as wave breaking, shoaling, refraction and reflection. The presence of all these processes at and on shore platforms have been successfully measured in the field.

Field measurements have continuously showed that the maximum wave heights and wave energies reach the platform during high tide [Ogawa et al., 2012] [Marshall and Stephenson, 2011][Ogawa et al., 2011]. Underlining the control of water depth on wave transformation on these landforms. A consequence of this is that larger waves, produced during storm events, tend to break further off shore, leading to out filtering of the highest energy waves. This has been concluded based on field measurements by Stephenson and Kirk [2000] and Marshall and Stephenson [2011]. Therefore it is not guaranteed that high energy conditions in deep water give a proportional increase in energy on the platform. Off shore structures, such as a low tide cliff, have been noted to cause breaking of larger waves and cause dissipation of energy [Stephenson and Kirk, 2000] [Marshall and Stephenson, 2011] [Trenhaile and Kanyaya, 2007]. In some cases the offshore bathymetry and water depth can have a huge influence. Stephenson and Kirk [2000] found that, due to refraction and shoaling, as little as 0.3-8.8% of the deep water wave

energy reaches the platform edge. With this said it is not unusual for unbroken waves to propagate onto the platform, such conditions have been found on many sites e.g.[e.g. Marshall and Stephenson, 2011, Poate et al., 2016, Trenhaile and Kanyaya, 2007]. In summary; when trying to understand the wave processes connected to a rock platform it is important to look at the conditions of the nearshore area off the seaward edge, as they are key to how the waves are transformed before they actually hit the edge of the platform and hence determine the characteristics of the waves working on the platform.

When looking at specific morphological or bathymetrical features the depth in front of the platform edge [Stephenson and Kirk, 2000], the elevation, width and slope of the platform [Marshall and Stephenson, 2011] have been identified as important. Marshall and Stephenson [2011] ranked the importance of these three factors with water depth being the most important, followed by platform gradient and lastly width.

3.3 The wave breaking index

A few studies on rocky platforms have looked at the the breaking index (γ_b), i.e. the relationship between wave height and water depth, and compared it to studies done on similar landforms such as coral reefs or beaches (see Table 1 for summary).

Table 1: Breaking index $\gamma_{b_{m0}}$ found in previous studies.

Study	$\gamma_{b_{m0}}$
Farrell et al. [2009]	0.6
Ogawa et al. [2011]	0.4
Ogawa [2013]	0.39-0.45
Ogawa et al. [2015]	0.4-0.6
Poate et al. [2016] (site 1)	0.3-0.5
Poate et al. [2016] (site 2)	0.3-0.5
Poate et al. [2016] (site 3)	0.2-0.4
Poate et al. [2016] (site 4)	0.4-0.6

The first study investigating breaking index on rocky shore platforms was done by Farrell et al. [2009]. The study showed that the value of $\gamma_{b_{rms}} = 0.42$ (approximately $\gamma_{b_{m0}} = 0.6$ if converted), first determined by Thornton and Guza [1982], for breaking of an irregular sea on a natural beach, is a good approximation for wave breaking across a rock platform. Ogawa et al. [2011] found a much lower value of $\gamma_{b_{m0}} = 0.4$. Similar results were concluded by Ogawa [2013] where the results showed a value of $\gamma_{b_{m0}} = 0.4$ just in front of the seaward edge and 0.45 and

0.39 when moving landwards on the platform. Slightly higher values were found by Ogawa et al. [2015], where a value of $\gamma_{b_{m0}} = 0.4$ was found on the central platform and 0.6 at the cliff toe. The latest study on the topic by Poate et al. [2016] investigated breaking index across four different platforms. The study found a rather narrow spread of values for the individual site. The variation between sites was however larger. Two platforms had similar values ranging from 0.3-0.5, whereas the other two platforms had values between 0.2-0.4 and 0.4-0.6 respectively: All values were confined by an upper level of $\gamma_{b_{m0}} = 0.6$.

In summary it can be said that the previous literature has showed a range of values between $\gamma_{b_{m0}} = 0.2 - 0.6$, with differences depending on studies and location on the platform. Ogawa et al. [2011] related the discrepancy with other studies to difference in bottom slope, platform characteristics, oceanographic conditions and analytic method. The study by Poate et al. [2016] confirms this by showing that rougher platforms tend to have a smaller breaking index and smoother, wider platforms tend to have values closer to that of beaches. The study by Ogawa et al. [2015] investigated the importance of bottom slope as a controlling factor by investigating the applicability of the empirical equation for γ_{max} as a function of slope by Nelson [1987]. The result showed very good agreement between observed and calculated values, indicating that bottom slope indeed is an important factor for wave breaking and breaking index.

Wave breaking is highly controlled by water depth and it is therefore natural to assume that any increase, or decrease, in water level will affect the position of breaking. The change in water level due to factors such as reflected waves, standing waves, or storm surge are hence important. This has been confirmed by, for example, Trenhaile and Kanyaya [2007], who recorded an increased water level during storm conditions which changed the breaking position of the incoming waves. Ogawa et al. [2015] is the first to measure wave setup on a rocky platform. The study showed that the setup during low tide, in storm conditions (18% of incident H_{m0}), is similar to the wave setup for planar beaches (17%) [Thornton and Guza, 1982]. The study also showed big variations in setup depending on tide. This indicates that there are underlying processes such as lateral flow and dumping of water onto the platform as a consequence of wave breaking at the seaward edge.

In conclusion there are many things controlling the position of wave breaking in front of and on a shore platform, therefore it is difficult to approximate the wave breaking index with only one number. Especially close to the cliff toe, where reflection of waves might be present and wave setup is in its max, a single number is not to be recommended [Ogawa et al., 2015].

3.4 Wave attenuation

Many studies on rock platforms have analyzed wave energy attenuation across the platform. Research has found that waves are efficiently attenuated on rocky platforms, i.e. a proportion of the wave energy is lost when moving across the platform. The specific details of this attenuation, i.e. how, how much and where most of the energy is lost depends on the characteristics of the platform.[e.g. Stephenson and Thornton, 2005, Ogawa et al., 2012, Beetham and Kench, 2011].

The exact amount of energy lost over the platform varies greatly between studies and it is therefore difficult to draw any conclusions about general trends. Stephenson and Kirk [2000] found that only 4.9-6.8 % of the incident wave energy reaches the landward cliff, i.e. almost all of the wave energy is dissipated. In the study by Ogawa et al. [2012] the results showed that as much as 7-60 % of the incident wave energy was found at the landward cliff. In Marshall and Stephenson [2011] study no significant loss in total spectral energy could be found, although a change to longer period waves did occur. Ogawa et al. [2012] related the discrepancy between studies to differing morphology and wave conditions, and specifically pointed out a higher elevation in combination with higher waves and a steeper slope at the site researched by Stephenson and Kirk [2000] compared to their field site.

The fact that the energy attenuation varies so greatly between studies but also on a specific site can be explained by the fact that wave energy is related to wave height squared and is very much affected my wave breaking [CEM, 2002]. Therefore the same controlling factors as for wave height and wave breaking, apply here. Field measurements have shown that both tidal level, platform morphology, including slope and platform roughness [Poate et al., 2016], affect the proportion of wave energy transferred onto and across the platform [Marshall and Stephenson, 2011][Ogawa et al., 2012]. An example is the study of Trenhaile and Kanyaya [2007] which found that the wave attenuation decreases with increased slope and increased water height. In contrast Ogawa [2013] concluded that Type B platforms with a larger slope seem to be more dissipative than sub-horizontal platforms.

A very important morphological feature when talking about wave attenuation is the seaward edge of the platform. Here the water depth decreases rapidly inducing wave breaking on or close to the edge. Ogawa et al. [2011] presented that 40-80% of the wave energy is lost at the seaward edge, much like on coral reefs. The study by Ogawa et al. [2015] showed similar values of 40% and 60% wave attenuation at the seaward edge during low tide and high tide storm conditions, respectively. Both studies also discuss the importance of the platform elevation. Ogawa et al. [2015] compared the wave attenuation in relation to the relative edge submergence (h/H_{m0}) and found a negative relationship. The larger the edge submergence, the smaller the wave attenuation. Their results also indicated

that there seems to be a submergence threshold ($h/H_{m0} = 2.5 - 2.7$) where no wave dissipation takes place. This value is in line with values for coral reef platforms [Gourlay, 1994].

Another factor to take into consideration when looking at wave attenuation are the incident wave conditions. Ogawa [2013] investigated how differing offshore wave conditions, wind wave dominated or swell dominated seas, effect the waves on a rock platform. The main result showed that there was no significant difference between the two conditions, indicating that the wave processes on the platform are mostly controlled by morphology and water depth, not by incident wave characteristics.

Several studies have, on some sites, found an increase in wave height close to the landward cliff [Marshall and Stephenson, 2011] [Stephenson and Kirk, 2000]. This can be explained by the presence of reflected waves [Stephenson and Kirk, 2000] [Marshall and Stephenson, 2011] or the reformation of waves on deeper parts of the platform, which would undergo shoaling and breaking, leading to increased wave heights [Marshall and Stephenson, 2011].

3.5 Wave spectrum

Although the waves have, in most cases, gone through some transformation before reaching the platform, when looking at the waves just off the edge, the energy spectrum is generally dominated by offshore wave characteristics. This means that the wave field contains waves within the capillary, wind wave, swell and infragravity band with its dominance lying in gravity waves (GW) [Marshall and Stephenson, 2011, Ogawa et al., 2012, Stephenson and Kirk, 2000, Beetham and Kench, 2011, Ogawa et al., 2011]. The exact distribution between incoming wind waves, swell (both GW) and infragravity waves (IGW) naturally varies between studies, sites, local conditions and tidal state. A general trend can though be detected when going onto the platform and when moving further landward. All previous studies which have investigated wave transformation by looking at wave spectra have detected a filtering out of GW when moving across the platform. The GW dominated offshore wave spectrum switches towards a IGW dominant spectrum when moving in the landward direction, with the IGW peak at the cliff toe [Marshall and Stephenson, 2011, Ogawa et al., 2012, Stephenson and Kirk, 2000, Beetham and Kench, 2011, Ogawa et al., 2011, 2015]. It has been suggested that the underlying process for this is the release of group-bound, long period waves during the initial breaking of the waves [Ogawa et al., 2012] and the non-linear interaction of waves after breaking [Marshall and Stephenson, 2011]. As stated previously, wave breaking tends to occur before, at or just after the seaward edge of the platform, leading to the switch between GW and IGW usually occurring around the seaward edge. This switch between different wave types can

also be described as a dissipation of GW and an amplification of IGW across the platform. The studies clearly show a trend of an absolute increase in IGW height at the cliff toe [Beetham and Kench, 2011, Ogawa et al., 2012]. It should be mentioned that Ogawa et al. [2015] found a contradicting wave spectrum where the maximum IGW energy was found at the seaward edge, the spectrum was however still dominated by waves in the GW band.

Beetham and Kench [2011] as well as Ogawa et al. [2012] detected a rather rapid increase of IGW energy during the last 50 m of the platform, preceded by an almost stable IGW energy level across the middle part of the platform. This is explained by the presence of a ramp just before the landward cliff leading to increased shoaling and a nodal structure and standing waves on the central part of the platform [Beetham and Kench, 2011]. This agrees with Ogawa [2013] finding that a type B platform with a larger gradient seems to have a larger increase in IGW height across the platform when compared to a sub-horizontal shaped platform. The study by Beetham and Kench [2011], additionally, suggests that a wider platform would have a larger increase of IGW due to a greater distance for shoaling processes to act [Beetham and Kench, 2011]

To determine if wave characteristics or morphological features are the key controlling factor of waves on rocky shore platforms, some studies have looked at how incident waves affect wave transformation on the platform. Beetham and Kench [2011] and Ogawa et al. [2012] investigated the relationship between incident significant wave height and IGW height at the cliff toe. The two studies showed contradictory results, where Beetham and Kench [2011] found a strong correlation between incident waves and IGW height for both platforms studied. Ogawa et al. [2012] on the other hand found no correlation on their platform for waves in the infragravity band, whereas GW showed strong correlation with incoming waves. Ogawa [2013] investigated if offshore wave characteristics, wind wave dominated or swell dominated sea, had an effect on onshore platform wave transformation and found no significant difference for neither GW nor IGW.

Ogawa et al. [2015] studied the relation between GW and IGW and other external factors such as edge submergence, tidal level and the effect of storm conditions. The research showed a strong dependence on relative edge submergence with a clear threshold between IGW-dominance and GW-dominance. IGW dominate the wave spectra for lower edge submergence values whereas GW dominate if the relative edge submergence is higher. In short this means that there is a threshold where the water level at the edge is high enough for GW to dominate. Secondly the study suggests that tidal level is a strong controlling factor for IGW. In fact, there was almost no IGW energy present on the platform during low tide due to reflection of long period waves at the seaward edge. Thirdly when looking at the incoming wave energy, the conclusion was that although the absolute amount of IGW energy was in its maximum during storm conditions, the rela-

tive amplification of IGW over the platform was the highest during low energy conditions (30-80%). Another factor important for IGW is bottom friction. A study by Van Dongeren et al. [2013] on a coral reef showed that the dissipation of IGW due to bottom friction is greater on a rougher landform, compared to a smooth beach where nonlinear energy loss is more common [Henderson et al., 2006]. Similarly Pomeroy et al. [2012] found that bottom friction is important for the dissipation of waves across a reef flat, although the shorter GW lost more energy due to this process compared to the longer IGW. Both studies also observed a strong control on IGW by changes in water depth due to tidal variations. This was concluded to be primarily due to the variations of the magnitude of bottom friction due to water level [Van Dongeren et al., 2013][Pomeroy et al., 2012].

In the literature review for this report no previous investigation of the process of generation for IGW on rocky shore platforms was found. Research has though been conducted on beaches and to some extent on coral reefs. Both generation of IGW through the release of bound long waves, i.e. waves formed through nonlinear interaction of sea/swell waves which are amplified through shoaling and released through breaking in the nearshore zone, and IGW generation through breakpoint forcing, i.e. due to the time-varying oscillation of the location of the GW breakpoint, have been found in the research. The generation through the release of bound long waves is more likely to occur on mild sloping beaches [Masselink, 1995, Janssen et al., 2003]. On beaches it has been found that with increasing slope it is increasingly likely that breakpoint forcing is be the dominant process behind free IGW [Battjes et al., 2004][Baldock, 2012]. For reefs with a steep fore reef this point has successfully been validated by Pomeroy et al. [2012] and Van Dongeren et al. [2013] which found breakpoint forcing to be the origin of IGW propagating on the reef flat.

An interesting consequence of the presence of long period waves close to the cliff toe is their ability to be reflected. This has been measured by Ogawa et al. [2012] who did a directional analysis of waves on the platform and by Poate et al. [2016] who discovered wave breaking indexes, γ_b, above 1, leading to the conclusion that reflection of IGW must be present. Reflected waves effect the water level on the platform and hence affect the size of waves propagating along the landform as well as the location for wave breaking and is therefore an important process on a rocky shore platform.

4 Field Measurements

In this chapter the field site will firstly be introduced, followed by a description of the experimental setup and procedure.

4.1 Field site

Measurements were taken on and off a rock platform close to Cape Paterson, approximately 110 km southeast of Melbourne, Victoria (see Figure 11 and 12 for location).

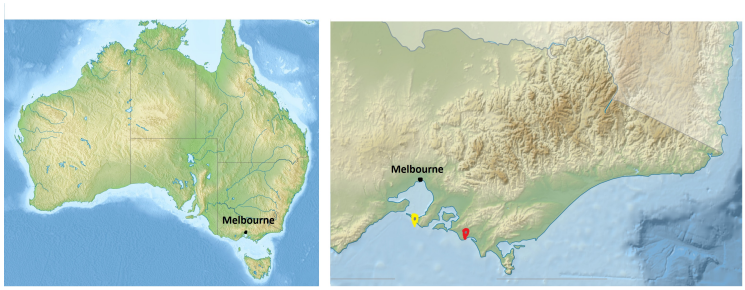

Figure 11: Location of field site (at red marker) and location of Point Nepean wave buoy (at yellow marker) [figure by Natural Earth Dataset under licence CC-BY-SA30]

Figure 12: Location of field site (at red marker)) [Google Maps, 2016]

The investigated platform is located in a small bay. The platform has a length of 550-700 m and is around 100-180 m wide. On the western side of the bay, a narrow part of the platform, around 80-90 m wide, extends further, an additional 200 m, offshore. The slope is close to horizontal for the whole platform (around 0-0.2 degrees). The shape of the seaward edge varies over the width of the platform, with more gentler sloping drop offs at the eastern side of the platform and more abrupt and complex edges at the western side (see Figure 13 for and Figure 15 for a picture of the area). Even though the platform is not continuously fronted by a clear steep drop off, characterizing a type-B platform, it is still defined as such, due to its horizontal orientation. On the landward side of the platform a beach is present. The substrate on the platform alters between being smooth and covered by organisms and plants to being very uneven with small boulders (see Figure 15 and 16). The orientation of the platform is 45° clockwise from a south to north orientation.

The surroundings and offshore bathymetry can be seen in Figure 13. Elevation profiles for the platform separately and for the platform and offshore area are shown in Figure 14. The offshore profile runs through the offshore transect and the platform profile runs through the measurement locations on the platform. The water depth decreases gradually when moving off shore and reaches depths of around 20 m. The bottom substrate mostly consists of vegetation covered smooth limestone ridges with occasional bare, sandy patches or canals. The most prominent feature in the nearby surroundings is the headland to the west of the field site, called Eagle's Nest, and the shallow area surrounding it.

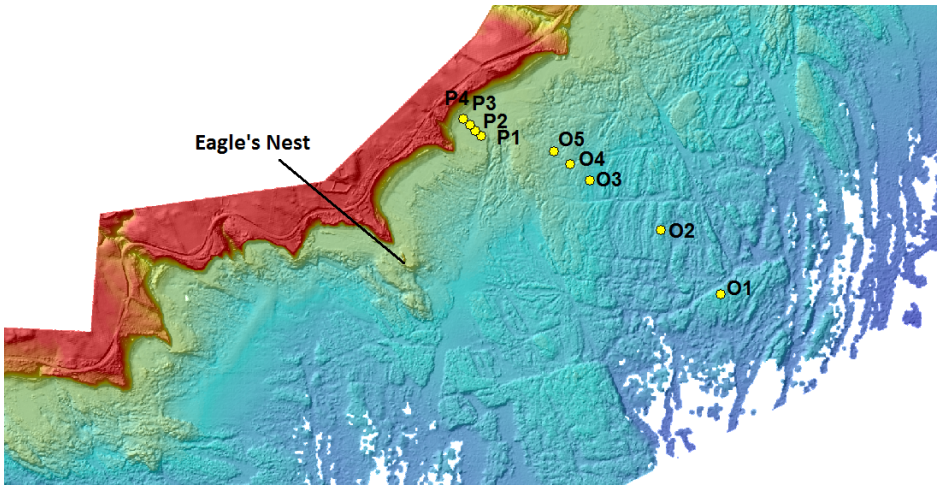

Figure 13: Bathymetry and location of measurements at field site.

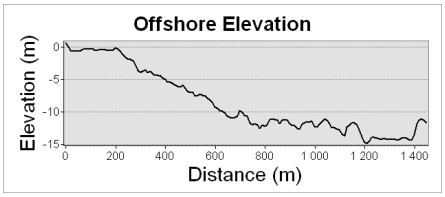

(a) Platform transcect

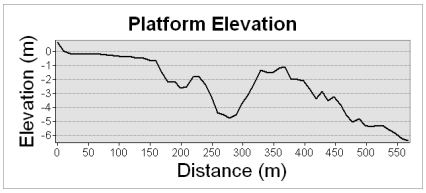

(b) Offshore transect

Figure 14: Elevation profiles for the platform and offshore transect

Figure 15: Picture of the rock platform at the field site.

The site is generally affected by waves approaching from the south west with varying wave heights (see Figure 18 for a common case of wave predictions by the Australian Bureau of Meteorology). The coast has a tidal variation of around of 2.1 m (mean high and low water spring tide) and 0.7 (mean high and low water neap tide) [Commonwealth of Australia-Bureau of Meteorology National Tide Centre, 2013].

4.2 Experimental setup and procedure

Waves were measured by nine RBR-2050 TWR pressure transducers which were deployed both offshore and on the platform. Offshore measurements were taken at 5 locations (O1-O5) over a period of 8 days (a period of 191 hours and 43 min)

Figure 16: An example of the substrate of the rock platform at the field site.

Figure 17: One of nine deployed pressure transducers.

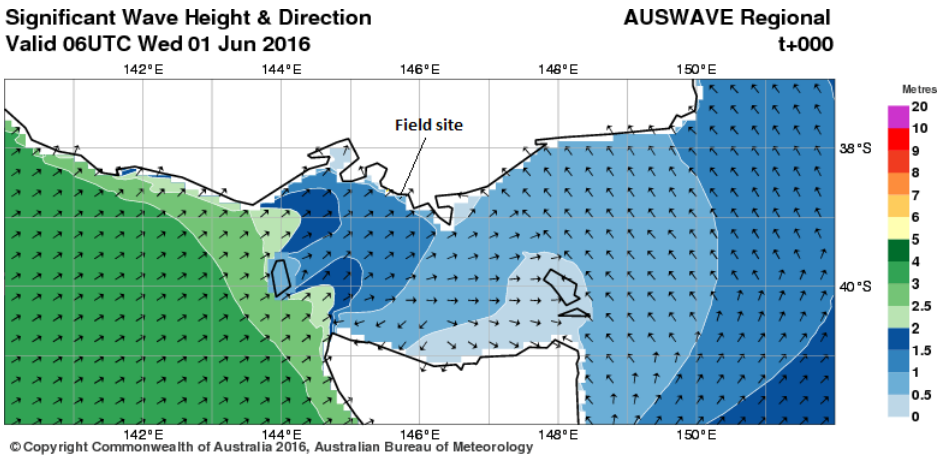

Figure 18: Typical wave conditions on the studied coast [Image by the Australian Bureau of Meteorology]

Table 2: Mean water level and distance from shore for measurement sites

Location	O1	O2	O3	O4	O5	P1	P2	P3	P4
h (m)	10.7	11.1	9.6	7.0	5.1	0.4	0.21	0.17	0.09
distance from shore (m)	1430	1030	630	510	410	110	80	40	0

between February 24 and March 3, 2016. On the platform, waves were measured at four locations (P1-P4), over a period of 22 hours and 57 min on 29 February and 1 March, 2016. For the location of the deployed wave sensors and water depth for the measurement locations, see Figure 13 and Table 2. Figure 17 shows a deployed wave sensor at the bottom substrate.

For the analysis, steady state ocean conditions were assumed for a period of 17 min and data was therefore collected continuously in bursts of 17.01 min with a sampling rate of 4 Hz.

The time-series of pressure was converted to sea-surface elevation by using a linear transfer function [Tucker and Pitt, 2001]. Spectral analysis was performed using fast Fourier transformation by Welch's averaged modified periodogram method of spectral estimation (see section 2.1.3 for a detailed description of the method). Every burst of 1024 samples was analyzed with a 256-point Hamming's window with a 50% overlap, giving 16 degrees of freedom (DOF).

Significant wave height and peak period as well as significant wave period was calculated from the variance spectrum according to Equations 5 and 6.

Total wave energy was calculated from the wave spectrum for every burst as well as separately for the GW band (0.05-0.33 Hz), with the subdivision of swell waves (0.05-0.125 Hz) and wind waves (0.125-0.33 Hz), and the IGW band (<0.05 Hz) according to the classification by Kench et al. [2009].

4.3 Results and Analysis

In this section the characteristics of the measured waves will first be presented and analyzed in regards to previous literature. Then the results of the modeling will be investigated and compared with the infield measurements.

The offshore measurements were taken over a period of 16 high tides and 15 low tides. The average tidal range during the measurement period was 1.2 m. On platform measurements were taken over a period of two high and low tides. The platform is exposed during low tide. The mean water depth, h, for each burst at the different locations can be seen in Figure 19.

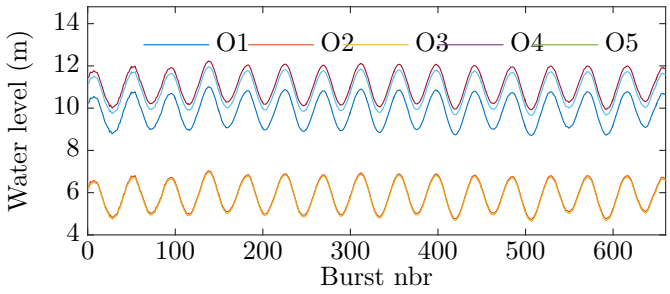

(a) Offshore locations.

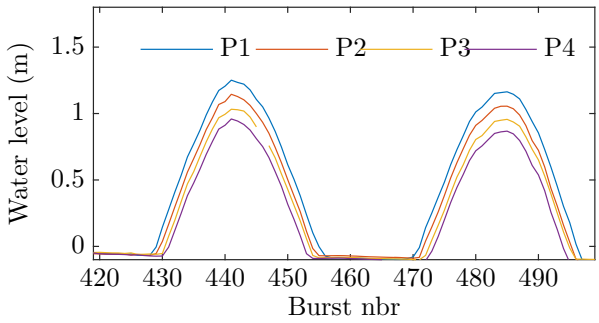

(b) Platform locations

Figure 19: Mean water depth, h, for each burst

4.3.1 Offshore wave conditions

The significant wave height, H_{m0} and period, T_s, for the offshore measurements are presented in Figure 20 and 21.

There are a few conclusions to be drawn from this. Firstly it can be seen that differing wave conditions have been detected during the experiment. Stormier conditions occurred between around burst 170 and 280, with significant wave heights up to 2.75 m, as well as calm seas with wave heights below 1 m towards the end of the time series. When looking at the wave period it can be seen that most waves have a significant period between 10-14 s with some exceptions. Lower significant periods were detected during the period just before the storm and just before the end of the time series. This could be due to increased winds during this time, leading to the build-up of larger waves shortly after. Shorter period wind waves would therefore be present, drawing down the significant wave period. When looking at the wave spectrum for bursts within these regions this

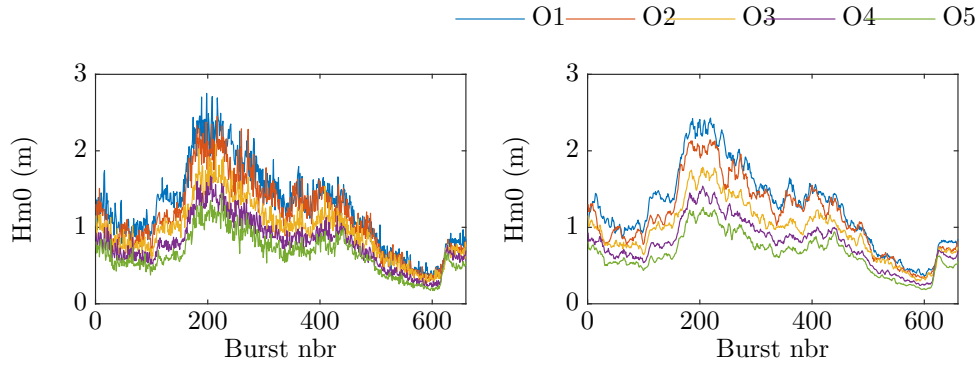

Figure 20: Measured H_{m0} for offshore sites. Actual values for every burst are shown on the left and smoothed data on the right.

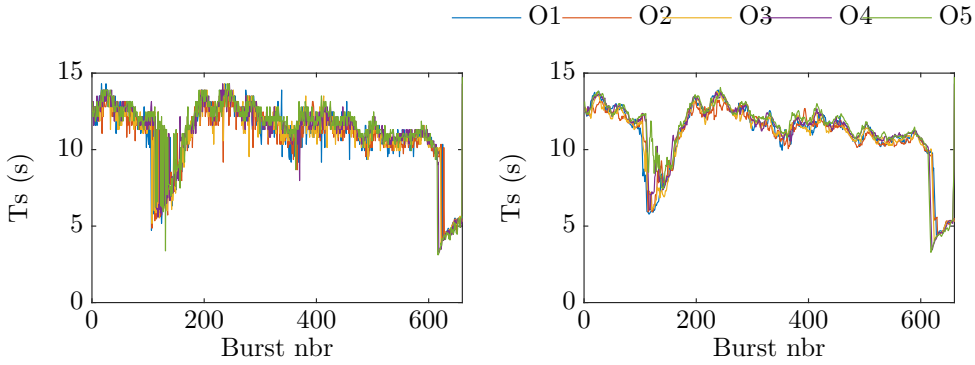

Figure 21: Measured T_s for offshore sites. Actual values for every burst are shown on the left and smoothed data on the right.

explanation can be verified by the presence of a second peak located within the wind wave frequencies, in addition to a peak around the typical swell frequencies, see Figure 27 for spectrum of burst 125 (found under spectral analysis section).

The incoming waves have an angle of between 180° and 217°, clockwise from north, corresponding to $\theta = 45°$ to $\theta = 82°$ (see Figure 22), where θ is the angle measured counter clockwise from a propagation direction which is perpendicular to shore. This means that the waves for the whole period move into the nearshore area with a large angle, in some cases, the waves propagate almost parallel to

shore. Generally it can be seen that the largest angles are found at the beginning of the time series with smaller incoming angles later on. An exception is the short increase around burst 560-600, see Figure 22.

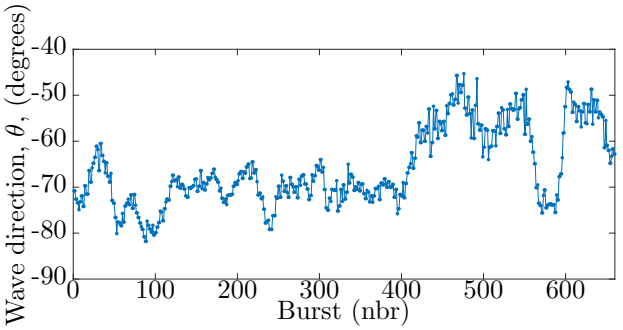

Figure 22: Recorded wave direction, θ, for incipient waves. Data collected by Port of Melbourne wave rider buoy.

4.3.2 Offshore wave transformation

When looking at the change in significant wave height and period between the different offshore locations some trends can be detected. Firstly it can be noted that there is no significant change of T_s between the different offshore locations (see Figure 21).

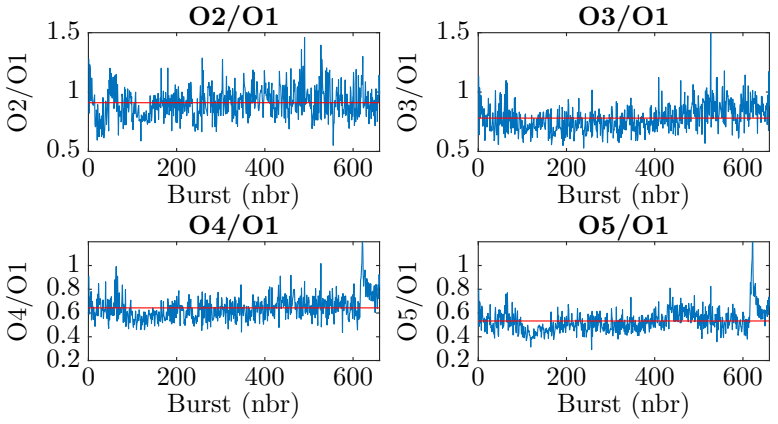

Figure 23: Proportional change of measured H_{m0} between most offshore location, O1, and remaining offshore locations

Table 3: Difference in measured significant wave height, H_{m0}, between offshore sites, expressed as fractions

Relationship between:	Suceeding sites				Incoming waves			
	O2/O1	O3/O2	O4/O3	O5/O4	O2/O1	O3/O1	O4/O1	O5/O1
Fractions	0.91	0.87	0.83	0.83	0.91	0.78	0.64	0.53

Figure 23 and Table 3 shows the proportional change of H_{m0} for the different sites, both in relation to the incoming waves measured at O1 and to the preceding site. The significant wave height is continuously decreasing when moving closer to shore. It can be seen that the two outer most probes have a rather small change, which can be explained by the fairly large water depths and distances from shore leading to that nearshore processes have not yet greatly affected the incoming waves. An average decrease in wave height has though been recorded between these two locations. This can be explained by the fact that long period waves interact with the bottom already in moderately deep water, leading to that the incoming waves are not completely unaffected by nearshore processes. The limit for when waves start interacting with the bottom is known to be at a depth of L/2 m [CEM, 2002]. According to linear wave theory the deep water wave length can be obtained as stated in Equation 8 [CEM, 2002].

$$L_0 = 1.56T^2 \tag{8}$$

According to this relationship, the shortest period waves in the time series start interacting with the bottom at a water depth of around 19 m. All measurement sites are located in water which is shallower than this threshold, hence all recorded waves are affected by the bottom already at the most offshore location.

The bottom substrate at the site is characterized by ridges of smoothed limestone, which has obvious signs of abrasion through the movement of sand across the substrate. This underlines the conclusion that waves interact with the bottom substrate already this far out from shore.

It is important to remember that the large angles of the incoming waves lead to that the path of wave propagation is not represented by the measurement transect. Instead, if for example the waves move parallel to shore, then the same wave crest will reach the probe locations at approximately the same time. This means that if there are differences between the locations it does not represent the wave transformation occurring between the different measurement points, instead it means that the same original offshore wave has gone through differing transformations before reaching the specific location. Therefore, the difference in wave height between O1 and O2 is not because the waves have travelled the distance between the locations further. Instead the underlying reason must be

due to that the processes affecting the incoming waves, before they hit the measurement locations, are different. Even though the water depth is similar at these two locations, O1 is situated in slightly shallower waters. When looking at the surrounding bathymetry it can be seen that O1 is located on a shallower plateau surrounded by deeper waters (see Figure 24). It is therefore likely that the waves undergo some shoaling and refraction, focusing energy onto this area, an effect that would be smaller for the waves propagating towards O2, where more even depths are found in the surroundings, leading to slightly higher values at O1.

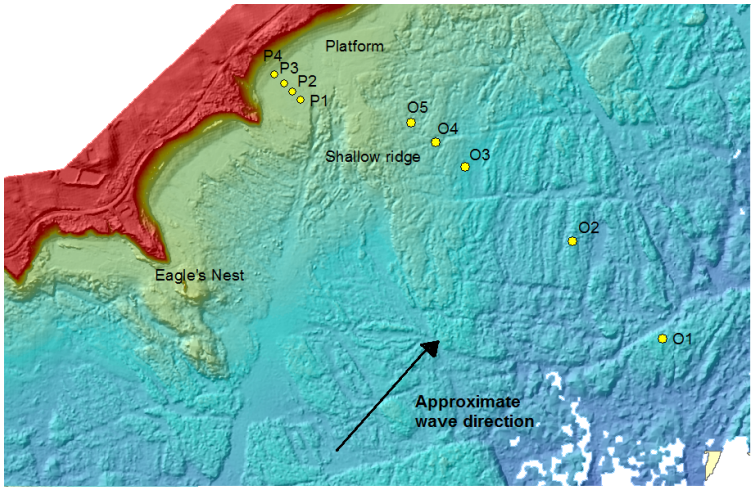

Figure 24: Bathymetry of field site with shallow areas and approximate wave direction marked out

When moving between O2 and O3 the decrease in wave height is larger even though the distance is similar to the one between O1 and O2 and the water is only approximately 1 m shallower, around 10m. When moving even closer to shore, the wave height continues to decrease with a similar rate between O3-O4 and O4-O5, this even though the distances are short and the water depth still is around 6 m. Especially between O4 and O5 there is no difference in depth, but a decrease in wave height has occurred. This larger than expected decrease of wave height at the three inner most locations can be explained by the presence of shallow water processes, such as refraction, diffraction and wave breaking which dissipates and changes the wave energy [CEM, 2002] [Holthuijsen, 2007]. The large incoming angles in combination with the complex bathymetry of the surroundings, lead to that these processes are very important. A ridge, with mean water depths of 1-3 m, extends out from the platform southwest of O5 at

a distance of approximately 100 m. In addition, a narrow shallow area, called Eagle's Nest, is located approximately 700 m further down the coast (see Figure 13). This ridge and Eagle's Nest is in line with locations O3-O4 for waves with extremely large angles. The shallow areas would cause waves to refract, diffract and break around these parts and hence give some shelter to the three inner most locations. This 'protection' effect would increase when moving closer to shore, explaining the decrease in wave height.

The largest absolute decrease in wave height between sites is found for the highest wave heights, whereas the lowest wave heights only show a small absolute decrease when moving shoreward, see Figure 20. When investigating the proportional decrease of wave height, see Figure 23, no such trend can be detected. Some other trends can though be discussed. For the three most shoreward locations slightly lower proportional decrease can be detected after burst 400.This corresponds to the decrease in wave direction around this burst. Smaller incoming angles would lead to a decrease of the effect of Eagle's Nest and the shallow ridge on waves reaching O3-O5 and lead to a smaller decrease at these sites. For O4 and O5, a larger decrease in wave height can be detected just after burst 100. This coincides with the decrease in significant wave period around the same time, see Figure 21. As mentioned previously, this decrease in wave period is due to an additional peak in the wave spectrum at wind wave frequencies. Wind waves are locally produced and might propagate in a different direction than the incipient waves and can affect the wave transformation processes.

4.3.3 Offshore spectral analysis

Figure 25 shows the wave energy power spectral density for the five offshore sites. It can be seen that, for all sites, most of the wave energy is contained within the swell energy region (0.05-0.125 Hz). An increase of energy in the wind wave region (0.125-0.33 Hz) can be detected before and during the storm event. A pickup of wind wave energy is also present at the end of the time series, corresponding to the sudden increase of wave height at this point.

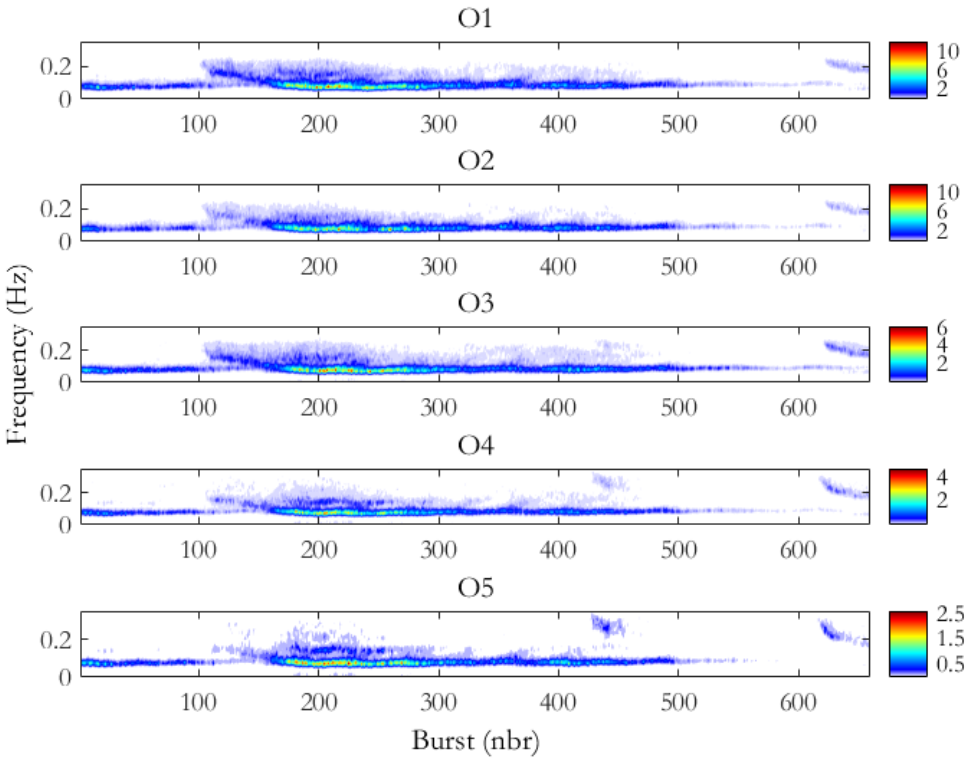

Figure 25: Spectral energy density for offshore sites.

When looking at the proportional distribution of wave energy between the different wave classifications (see Figure 26) the previously drawn conclusions are strengthened. It is clear that swell energy is dominant. Except just before the storm and at the end of the time series, where winds have picked up, but larger swell has not yet been built up.

Figure 27 shows the wave spectrum for a few individual bursts. It is shown that both clear swell dominated conditions (burst 310) as well as mixed conditions with energy peaks both at wind and swell frequencies occur during the time series (burst 125 and 210). Burst 125 occurs just before the storm waves are recorded, when the significant wave period is smaller and wind wave energy is dominant, this is clearly reflected in the wave spectra. Burst 210 is during the storm wave period and larger swell energies are recorded as well as a smaller wind wave peak, indicating that wind still produces smaller waves locally.

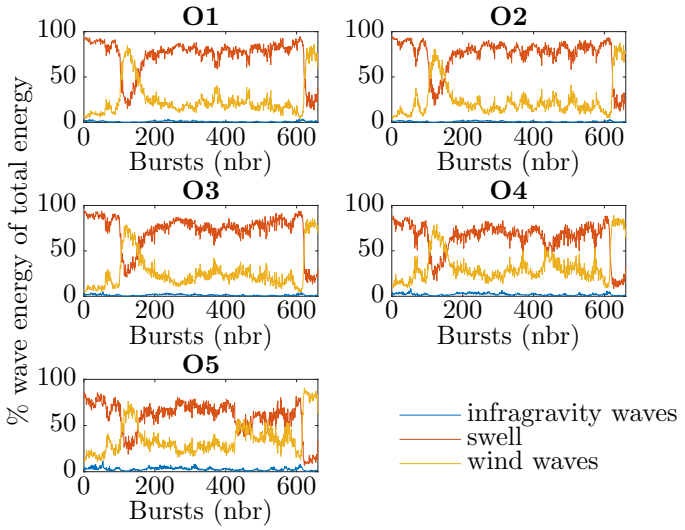

Figure 26: Distribution of wave energy of different classification in percent (%) of total energy at all offshore locations.

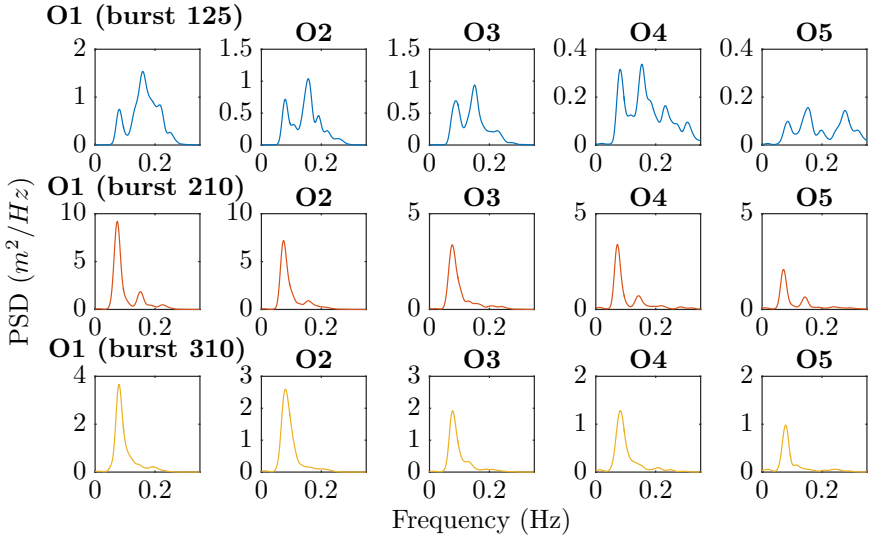

Figure 27: Wave spectrum for three different bursts (125 in blue, 210 in red, 310 in yellow) for all offshore sites

4.3.4 Platform wave transformation

The measured values for significant wave period, T_s, on the platform generally lie between 6-8 s with no clear trend or significant difference between sites.

Figure 28 shows H_{m0} for the four platform locations. It can clearly be seen that the wave height on the platform is strongly controlled by the tide, i.e. the water depth on the platform, whereas the offshore wave height is not (see Figure 19a). When moving across the platform, H_{m0} decreases slightly, all though there is no significant difference between the inner most locations. The decrease could be due to that water depth decreases towards the shore as well as energy dissipation through friction or as a consequence of other morphological features on the platform [e.g. Stephenson and Thornton, 2005, Ogawa et al., 2012, Beetham and Kench, 2011]. The smaller decrease between the two inner most sites could be due to the reformation of waves on deeper parts of the platform, which would undergo shoaling and breaking, leading to increased wave heights [Marshall and Stephenson, 2011].

The large difference between the inner most offshore location and the platform measurements indicates that waves on the platform have broken and reformed before reaching the first location on the platform.

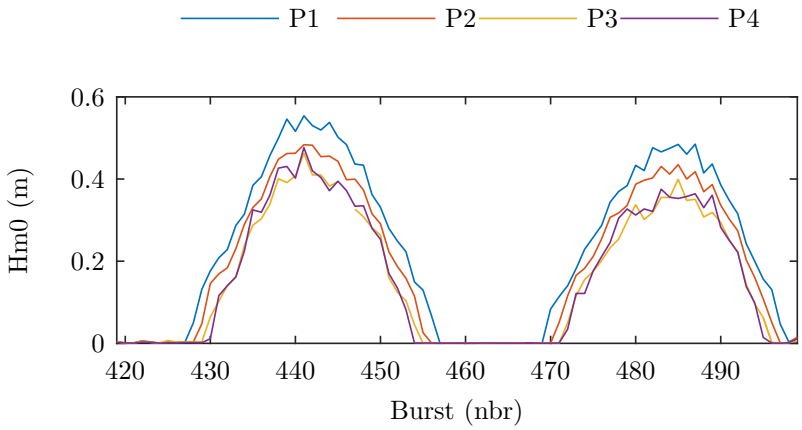

Figure 28: Measured H_{m0} for platform sites.

Figure 29 shows the relationship between H_{m0} and water depth h; the breaking index $\gamma_{b_{m0}}$. The good fit of a linear regression line for all locations separately, as well as combined, underlines the conclusion that the main underlying factor determining wave height on the platform is tidal level i.e. water depth. The

values for $\gamma_{b_{m0}}$, (between 0.31-0.34) are within the range but slightly lower than the average result from previous studies by e.g. Ogawa et al. [2011], Farrell et al. [2009] and Poate et al. [2016] (see Table 1). The offset of the linear regression could be due to an inaccurate estimation of the barometric pressure, leading to consequences when deriving the water depth from the pressure sensors. This conclusion is strengthened by the fact that the water level for the platform locations is slightly lower than zero for low tide values (see Figure 19b).

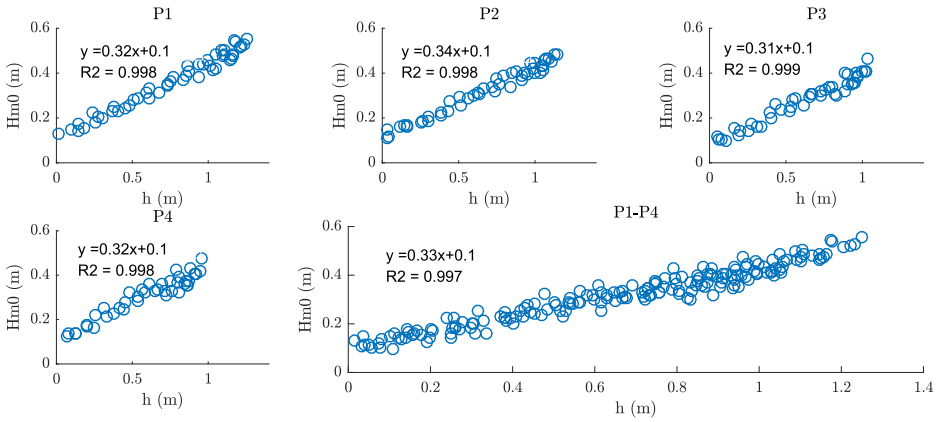

Figure 29: Linear regression relationships between wave height,(H_m0), and water depth, (h), for platform sites separately and together.

4.3.5 Platform spectral analysis

Figure 30 shows the wave energy power spectral density for the four platform locations. The wave energy at these locations is more spread out over all frequencies compared to the offshore locations (see Figure 25). For all sites, wave energy is contained both in the wind wave, swell and infragravity wave band. It can be seen that the clear swell peak at P1 decreases towards P4. An opposite trend is seen for IGW energy, were an increasingly clear peak is present closer to the landward edge of the platform.

Figure 31 shows the relative proportions of spectral energy contained within the different types of waves. The shorter wind waves are dominant for all cases, this can be explained by the fact that low intensity was detected for the whole wind wave spectrum, leading to a larger total energy, compared to the higher smaller peaks within the swell or IGW band. Another trend is that the second most dominant type of wave energy stems from swell for P1 and P2 and from IGW for P3 and P4.

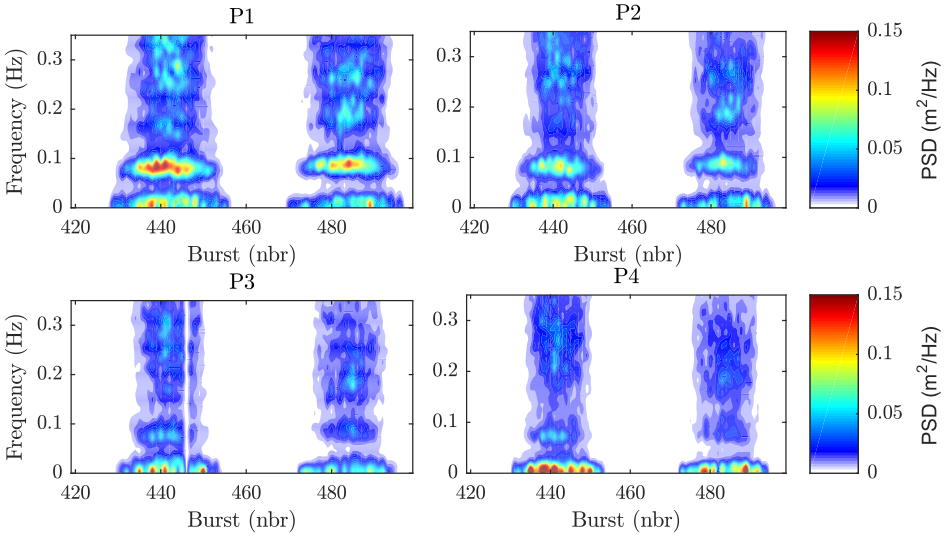

Figure 30: Spectral energy density for platform sites.

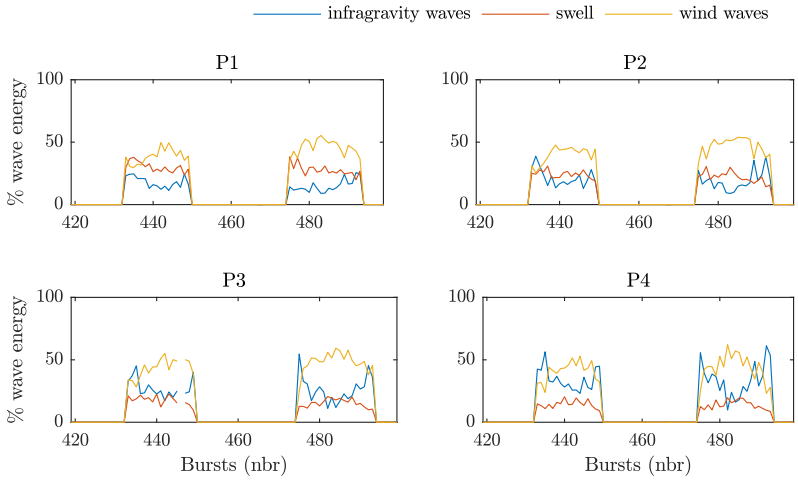

Figure 31: Distribution of wave energy of different classification in percent (%) of total energy at platform locations.

The results from the spectral analysis for the platform differ from what has been found by previous research. Most other studies have shown that IGW are formed during the propagation of waves across the platform [e.g. Ogawa et al., 2011]. Here these type of waves are present already at the beginning of the platform. The dominance of IGW is though increasing across the platform, towards the landward edge, with the largest increase between the two most landward locations a trend previously documented [e.g. Ogawa et al., 2011, Beetham and Kench, 2011]

5 Model Theory and Implementations

5.1 Theoretical formulation

The model used in this report is a multi-directional random wave transformation model (EBED), based on the wave energy balance equation, originally developed by Mase [2001] and modified by Nam et al. [2009]. In this section the concept behind the wave energy equation is firstly explained in more detail, before a general description of the modified EBED model is presented.

5.1.1 The wave energy balance equation

In this section the energy balance equation for a random phase/amplitude model is described. The random phase/amplitude model assumes that the water level elevation can be described as the sum of a large number of independent wave components with individual frequencies and directions. The energy balance equation therefore considers the change of the spectral density $E = E(f, \theta)$ for each wave component in time (t) and space (x,y), i.e. $E(f, \theta; x, y, t)$.

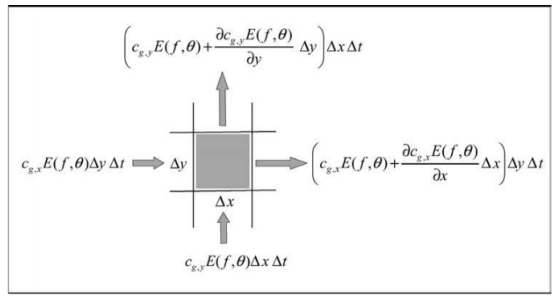

Figure 32: The concept of energy propagation through one geographic cell [Holthuijsen, 2007]

When deriving the wave energy balance equation we consider a geographic cell with a length Δx and a height Δy (see Figure 32). The energy balance for this cell, for one specific direction θ and frequency f, $E(f, \theta)$, for the time period Δt can then be described as:

$$change\ in\ energy = net\ import\ in\ energy + local\ production/dissipation\ of\ energy \tag{9}$$

The net import of energy, during the interval Δt, in the x-direction and y direction can be described as (also see Figure 32):

$$import\ of\ energy\ x\text{-}direction = c_{g,x}E(f,\theta)\Delta y\Delta t - (c_{g,x}E(f,\theta) + \frac{\delta c_{g,x}E(f,\theta)}{\delta x}\Delta x)\Delta y\Delta t = -\frac{\delta c_{g,x}E(f,\theta)}{\delta x}\Delta x\Delta y\Delta t \quad (10)$$

$$import\ of\ energy\ \text{-}direction = -\frac{\delta c_{g,y}E(f,\theta)}{\delta x}\Delta x\Delta y\Delta t \quad (11)$$

where $c_{G,x}$ and $c_{G,y}$ is the x component of the wave group velocity c_G and can be described as:

$$c_{g,x} = cos\theta \quad (12a)$$

$$c_{g,y} = sin\theta \quad (12b)$$

The locally generated or dissipated energy can be described as:

$$locally\ generated\ energy = S(f,\theta)\Delta x\Delta y\Delta t \quad (13)$$

where $S(f,\theta)$ is a source term which includes all effects of generation or dissipation of energy, such as wind, wave-wave interactions and white capping, per unit time and unit surface area.

The energy balance equation can now be written as:

$$\frac{\delta}{\delta t}E(f,\theta)\Delta x\Delta y\Delta t = -\frac{\delta c_{g,x}E(f,\theta)}{\delta x}\Delta x\Delta y\Delta t - \frac{\delta c_{g,y}E(f,\theta)}{\delta x}\Delta x\Delta y\Delta t + S(f,\theta)\Delta x\Delta y\Delta t \quad (14a)$$

$$\rightarrow \frac{\delta E(f,\theta;x,y,t)}{\delta t} + \frac{\delta c_{g,x}E(f,\theta;x,y,t)}{\delta x} + \frac{\delta c_{g,y}E(f,\theta;x,y,t)}{\delta y} = S(f,\theta;x,y,t) \quad (14b)$$

The equations above are applicable for deep water waves. When the waves move into shallower water other effects such as depth induced wave breaking and bottom friction, shoaling, refraction and diffraction will affect the wave energy and are therefore necessary to take into account. This is solved in a number of different ways. Effects such as wave breaking and bottom friction are simply incorporated into the source term, while shoaling is accounted for by using the depth-dependent group velocity. Diffraction and refraction are better dealt with by adding an additional propagation term to the energy equation. When a wave component reaches shallower water it changes direction, which leads to that the

energy density does not only travel in x- and y-space it also propagates through a θ-space. The energy equation for shallow waters has another dimension, θ.

The principle of the energy equation is the same as for deep water waves, described above, with the addition of another term, the directional energy, when describing the *'net import of energy'*. The directional energy for each wave component is described as a distribution across different directions, discretized into bins with the width $\Delta\theta$ see Figure 33

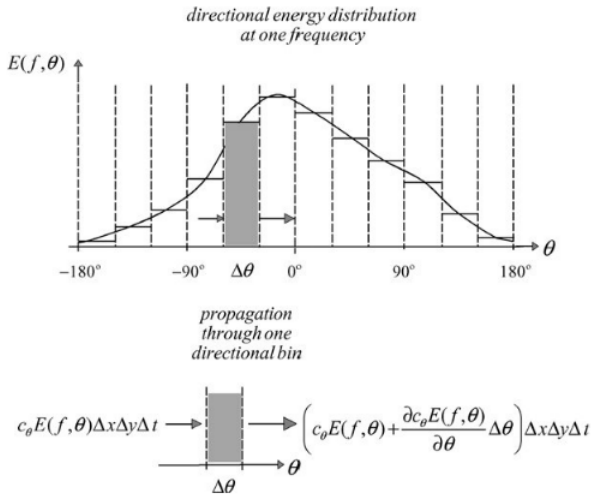

Figure 33: The directional distribution of wave energy at one location, one frequency, at one moment in time. The continuous energy shown as the solid line and approximated with directional bins. Turning of the wave direction, represented as propagation of wave energy through a bin in directional space is shown at the bottom. [Holthuijsen, 2007]

The net import of directional energy is then described as the energy import through the left hand side of the bin minus the energy export through the right side of the bin according to:

$$\begin{aligned} \textit{import of energy } \theta\textit{-direction} = c_\theta E(f,\theta)\Delta x\Delta y\Delta t - (c_\theta E(f,\theta)+ \\ \frac{\delta c_\theta E(f,\theta)}{\delta\theta}\Delta\theta)\Delta x\Delta y\Delta t = -\frac{\delta c_\theta E(f,\theta)}{\delta\theta}\Delta\theta\Delta x\Delta y\Delta t \end{aligned} \quad (15)$$

where c_θ is the rate of turning due to refraction or diffraction processes.

The total energy balance for shallow water is hence:

$$\frac{\delta E(f,\theta;x,y,t)}{\delta t}+\frac{\delta c_{g,x}E(f,\theta;x,y,t)}{\delta x}+\frac{\delta c_{g,y}E(f,\theta;x,y,t)}{\delta y}+\frac{\delta c_{g\theta}E(f,\theta;x,y,t)}{\delta \theta} = S(f,\theta;x,y,t) \quad (16)$$

This equation is the basis for the EBED model used in this report.

5.1.2 The modified EBED model

The EBED model is based on the steady state energy balance equation with energy dissipation and diffraction terms contained in the source term. The steady state governing equation is expressed as:

$$\frac{\delta(v_x S)}{\delta x}+\frac{\delta(v_y S)}{\delta y}+\frac{\delta(v_\theta S)}{\delta \theta} = \frac{\kappa}{2\omega}\left\{(CC_g cos^2\theta S_y)_y - \frac{1}{2}CC_g cos^2\theta S_{yy}\right\} - \epsilon_b S \quad (17)$$

Where S is the angular-frequency spectrum density (previously expressed as $E(f,\theta)$), (x,y) are the horizontal coordinates, θ is the angle measured clockwise from the x axis, ω is the frequency (previously expressed as f), C is the phase speed and C_g is the group speed, $(v_x, v_y v_\theta)$ are the propagation velocities in the different dimensions (previously $c_{g,x}, c_{g,y}$ and $c_{g,\theta}$). The source term on the right hand side of the equation contains a diffraction part, the first term, and a part representing the energy dissipation due to wave breaking, the second term. κ is a free adjustable parameter deciding the influence of diffraction effects and ϵ_b is the wave breaking energy dissipation coefficient.

The modification by Nam et al. [2009] entails an improved description of the term for energy dissipation caused by breaking. This it done with the aim to address the model's tendency to overestimate wave heights in the surf zone. The new approach of describing the energy dissipation is based on the model developed by Dally et al. [1985] and the adjusted steady state energy balance equation is as follows:

$$\frac{\delta(v_x S)}{\delta x}+\frac{\delta(v_y S)}{\delta y}+\frac{\delta(v_\theta S)}{\delta \theta} = \frac{\kappa}{2\omega}\left\{(CC_g cos^2\theta S_y)_y - \frac{1}{2}CC_g cos^2\theta S_{yy}\right\} - \frac{K}{h}C_g(S - S_{stab}) \quad (18)$$

where K is the dimensionless decay coefficient, h is the still-water depth and S_{stab} is the stable wave spectrum density, derived from the stable wave height H_{stab}. The stable wave height derived according to:

$$H_{stab} = \Gamma h \tag{19}$$

where Γ is a dimensionless empirical coefficient, similar, but not equal to the braking index γ_b. The stable wave height represents a wave field where wave breaking has occurred and has now stopped and does no longer affect the wave height. Whereas the breaking index is applicable for a situation where breaking processes are still present.

The model's main output consists of the significant wave height and wave period, H_{m0} and T_s as well as the mean wave direction $\overline{\theta}$. The input consists of the same parameters in addition to bathymetry and tidal data for the model area. The input wave parameters are used to produce a wave spectrum which is used for the energy balance equation.

5.2 Model implementation

The measurements at O1, the wave sensor located furthest from shore, where used as input wave data. Directional data, i.e. the weighted mean direction taken over waves of all frequencies in a given record period, was obtained from a wave rider buoy, owned by Port of Melbourne located off Point Nepean approximately 80 km north west of the field site (see Figure 11). A JONSWAP spectrum was assumed at the boundary conditions and produced using the input wave characteristics as well as the standard values for the spectral parameters, i.e. $\gamma = 3.3$, $\sigma_a = 0.07$, $\sigma_b = 0.09$ and $S_{max} = 25$.

The initial model runs for this project where run over an area covering only the bay of the platform with an orientation perpendicular to the shoreline. The area was then gradually increased to ensure that the transformation of waves with large angles was being covered. To compensate for the model's limitation when simulating wave propagation of waves with large angles, the bathymetry was, for some runs also, rotated towards the direction of incoming waves. The model simulations were analysed both spatially in two dimensions and by comparing the model output at the specific locations of the measurements. A spectral analysis of the spectrum produced and used my the model in comparison to the spectrum detected in the measurements was also done. To obtain the best model fit, many different scenarios where tested and analysed. After each run the result was analysed and the input conditions adjusted in order to investigate if the model is able to accurately reproduce the wave conditions detected in the measurements. The following four main ones will be presented in this report:

Model run 1
Area: The model was run over an area covering the extension of the bay and most of the bay to the west of the platform, and offshore until the location of

the furthest off shore wave sensor. A bathymetry grid with a grid size of 10 m x 10 m was extracted from ArcMaps using LIDAR data. The model area and its bathymetry is shown in Figure 34.
Orientation: Perpendicular to the coastline, rotated 45°clockwise from south to north orientation.
Input Waves: H_{m0} and T_s for the input waves were derived from the measurements at O1, where each burst represents one wave. Tidal level was calculated for each input wave by comparing the measured water depth at O1 with the water depth at the same location, extracted from the bathymetry grid. Directional data for the incoming waves was derived from Port of Melbourne wave buoy.

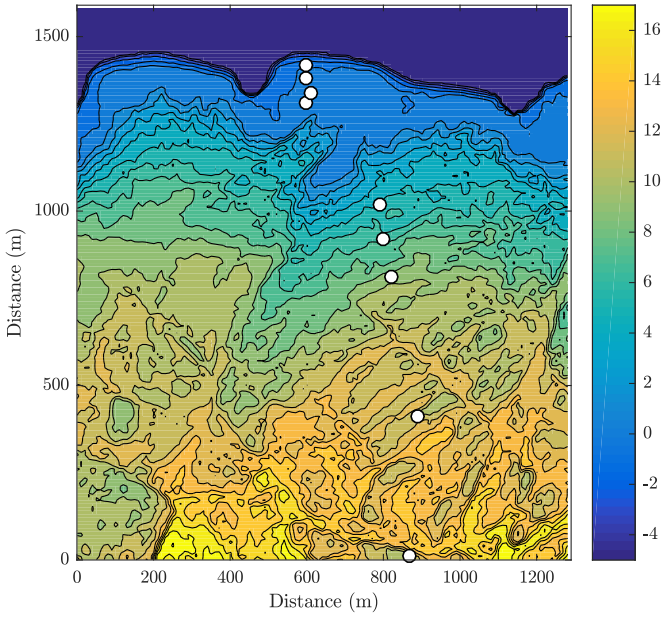

Figure 34: Model run 1: bathymetry of the model area. The locations of the field measurements are indicated by white dots.

Model run 2
Area: A larger area was used, covering the extension of the bay of the field site and approximately 2 km offshore and 3 km west along the coast. A bathymetry grid with a grid size of 10 m x 10 m was extracted from ArcMaps using LIDAR

data. The most offshore edge and the right corner of the model area did not contain depth data for every grid cell. An approximate value of 23 m was set for these offshore grid cells without data. The model area and its bathymetry is shown in Figure 35.
Orientation: No rotation from south to north orientation.
Input Waves: H_{m0} and T_s for the input waves were derived from the measurements at O1, where each burst represents one wave. Tidal level was calculated for each input wave by comparing the measured water depth at O1 with the water depth at the same location, extracted from the bathymetry grid. Directional data for the incoming waves was derived from Port of Melbourne wave buoy.

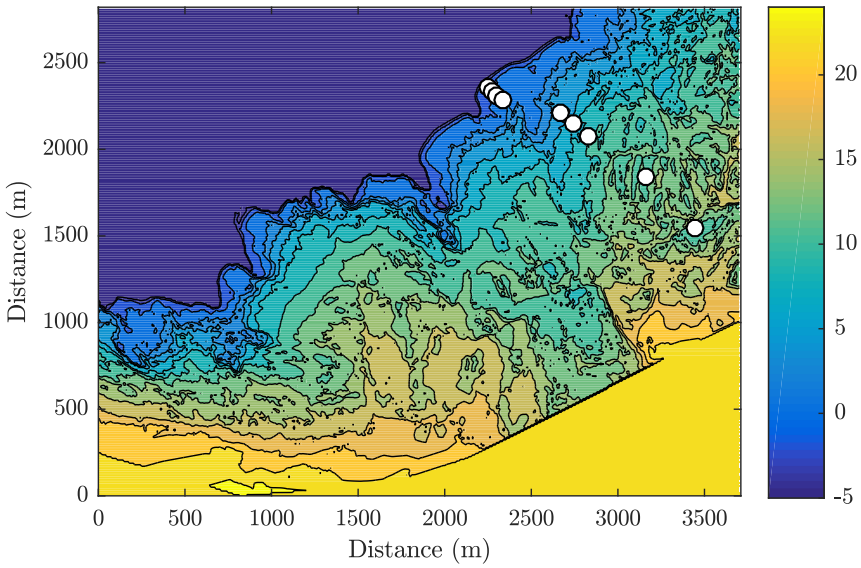

Figure 35: Model run 2: bathymetry of the model area. The locations of the field measurements are indicated by white dots.

Model run 3a and 3b
The same input conditions as for model run 2 were used but with increased directional data. To the measured incoming wave angle 25°(model run 3a) and 40°(model run 3b) were added.

Spectral analysis and model run 4a and 4b
The agreement between the standard JONSWAP spectrum used by the EBED

model and the spectrum produced by the field measurements has been evaluated. It is then investigated if the fit of the wave spectrum can be improved.

The shape of the JONSWAP spectrum can be adjusted by changing its parameters, one being the peakedness parameter, γ, which determines the concentration of the spectrum at the peak frequency. Instead of using the standard value, γ can be estimated, using T_p and H_{m0}, by a relationship based on qualitative considerations of deep water wave data from the North Sea developed by Torsethaugen et al. [1985] (see Equation 21).

$$D = 0.036 - 0.0056 * T_p / \sqrt{(H_{m0})} \tag{20a}$$

$$\gamma = exp(3.484 * (1 - 0.1975 * D * T_p^4 / (H_{m0}^2))); \tag{20b}$$

The peakedness parameter is adjusted in this way and two additional model runs, 4.a and 4.b, were performed. The remaining input values are set as for model run 3.a and 3.b, respectively.

5.3 Results and Analysis

In this section, the results from the three different model simulations will be presented and analysed.

5.3.1 Model run 1: small area with shore normal orientation

Offshore locations

When comparing the measured waves to the output of the model at the offshore wave probe locations, the agreement is rather good between the three outer most locations. The model is however significantly overpredicting for the two inner most offshore locations (see Figure 36).

The input of the model is equal to the measurements at O1. For this model run, O1 is located on the first row of the model output, i.e. only 10 m from the input. It is therefore expected that the agreement between model and measurements is good. Figure 36 shows that the model output at O1 is very precise although it is underpredicting slightly. The root mean squared error for O1 is $RMSE_{O1} = 0.130$ (see Table 4). This discrepancy is likely to partly be due to the fact that the model is not adapted for large angles, leading to loss in spectral energy. For O2, the underprediction of the model has increased with an error of $RMSE_{O2} = 0.205$. At O3, the model simulation agrees well with the measured values, with $RMSE_{O3} = 0.147$. At the two inner most off shore locations, O4 and O5, the model output is significantly higher than the measured values, increasingly so when moving closer to shore, $RMSE_{O4} = 0.364$ and $RMSE_{O5} = 0.473$. It is clear that the model has not been able to simulate the energy loss observed between the three most shoreward deep water locations.

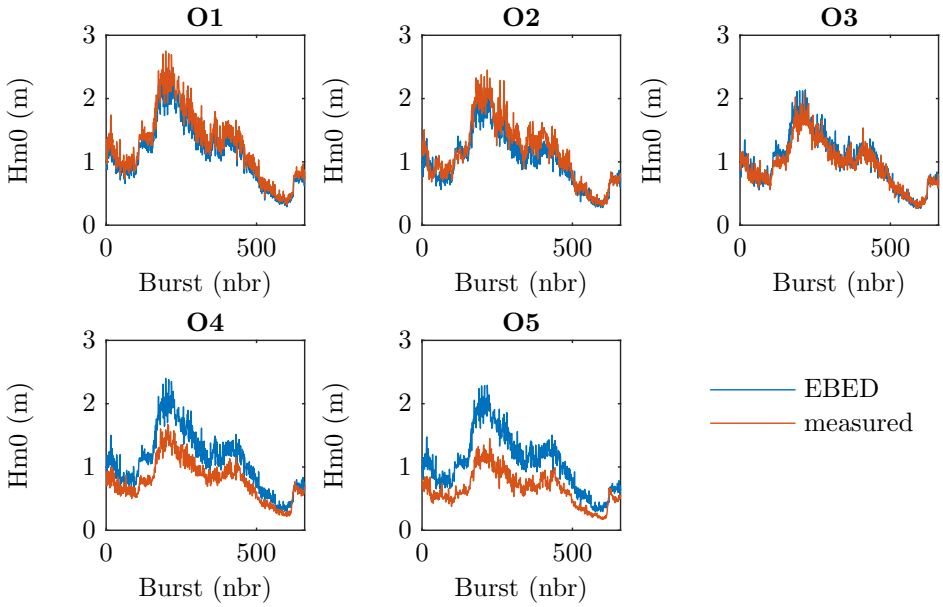

Figure 36: Result model run 1: modeled and measured values for significant wave height,H_{m0}, for all offshore location.

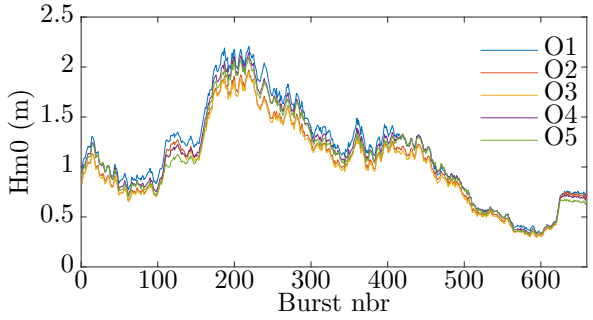

Figure 37: Result model run 1: modeled values for significant wave height,H_{m0}, for all offshore location.

Figure 37 clearly shows how the model has not been able to simulate the observed continuous decrease in wave height towards the shore. In fact the model

has only been able to reproduce a decrease in wave height between O1 and O2 whereas values for O2 and O3 are essentially the same. In addition, the simulations show an increase of wave height between O3 and O4/O5 (see Table 5). These discrepancies are likely due to that the model has not been able to simulate the nearshore processes, for this complex area, accurately. There are a few potential reasons for this. Firstly the area of this model run is too small to cover the shallow area around Eagle's nest and hence wave transformation processes connected to this morphological feature are not taken into consideration. Secondly, as mentioned previously, the model is not adapted for larger angles. When comparing the inputted wave directions to the output at O1 a large discrepancy can be detected (see Figure 38). This means that nearshore processes are poorly simulated as the modeled waves do not take the same path along the complex bathymetry as the real ones.

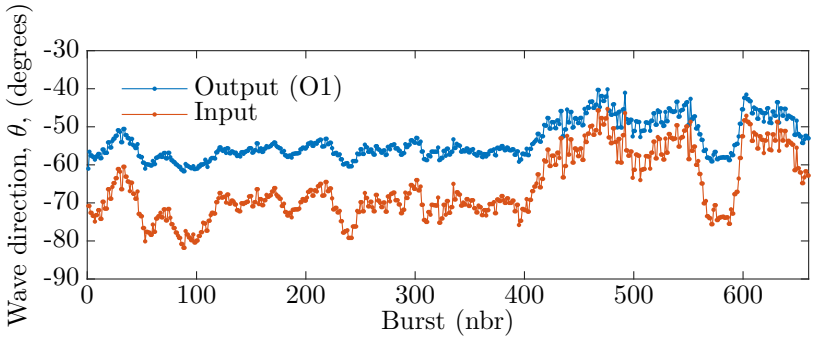

Figure 38: Result model run 1: Modeled wave direction, θ, on the first first row (at O1), compared to input values.

When looking at the 2D output of the model (see Figure 39), where the outputted wave height and wave direction is combined, this can clearly be seen. There are clear shoaling and refraction processes, where wave energy converges around the shallow ridge just to the left of O3-O5, leading to increasing wave heights occurring here. Processes caused by the complex bathymetry further down the shore are not covered by the area and the direction of the waves is more perpendicular to the shore than for the infield measurements.

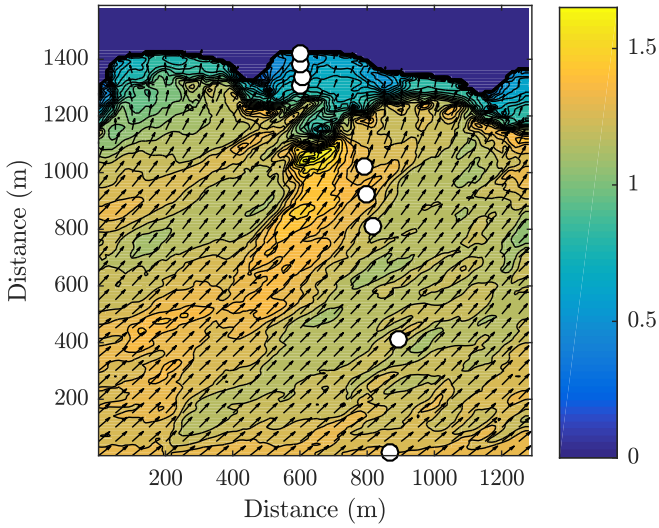

Figure 39: Result model run 1: Offshore wave transformation for burst 444, shown with wave direction (arrows) and H_{m0} (contours, scale to the right).

Platform locations

The modelled values for the locations on the platform follow the trend, of increasing wave height with increasing water depth, well. The peak wave height is though comparably higher than the measured values (see Figure 40). This can be explained by the fact that the observed relationship between water depth and wave height, $\gamma_{b_{m0}} = 0.33$, was noted to be lower than what is commonly found.

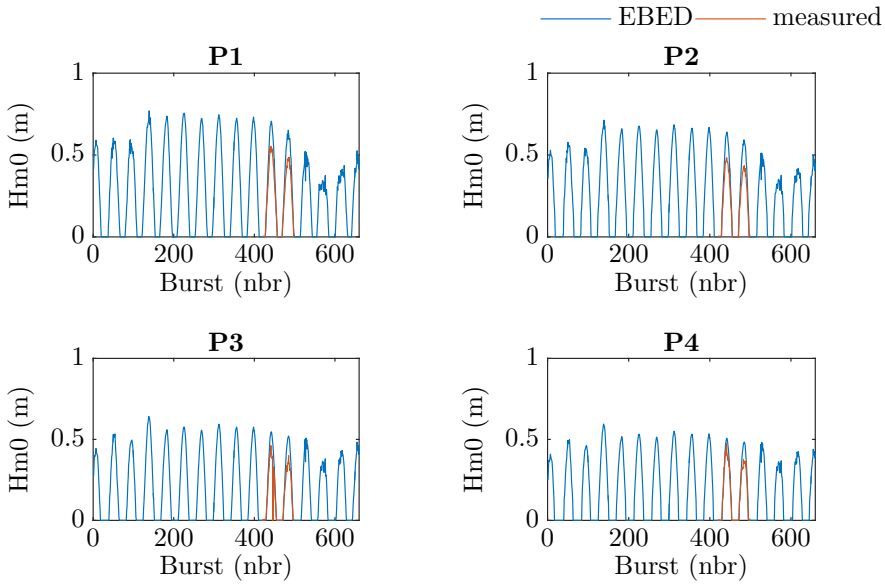

Figure 40: Result model run 1: modelled and measured values for significant wave height,H_{m0}, for platform location.

The inner most location, P4, has a slightly better fit than the other platform locations (see Table 4).

Table 4: Errors of model simulations, at all sites, expressed as root-mean squared error (RMSE).

		Location								
		P4	P3	P2	P1	O5	O4	O3	O2	O1
RMSE model run	1	0.0495	0.0894	0.0901	0.0927	0.4726	0.3645	0.147	0.2047	0.13
	2	0.0401	0.0802	0.0704	0.0907	0.5291	0.4237	0.2231	0.1726	0.1414
	3.a	0.0385	0.0781	0.0644	0.0775	0.3391	0.258	0.1403	0.2282	0.2514
	3.b	0.0338	0.07	0.0487	0.0547	0.1608	0.1272	0.1821	0.3258	0.358
	4.a	0.0375	0.0775	0.0632	0.0762	0.2916	0.2283	0.1408	0.2255	0.2552
	4.b	0.0293	0.0293	0.038	0.0457	0.1228	0.1697	0.277	0.4028	0.421

Table 5: Difference in significant wave height H_{m0} between offshore sites expressed as fractions.

Fractions		Measured	Run 1	Run 2	Run 3.a	Run 3.b	Run 4.a	Run 4.b
Succeeding sites	O2/O1	0,91	0,90	0,95	0,95	0,93	0,96	0,90
	O3/O2	0,87	0,98	1,01	0,99	0,94	0,97	0,90
	O4/O3	0,83	1,09	1,04	1,01	0,97	0,98	0,94
	O5/O4	0,83	0,97	0,98	0,95	0,93	0,93	0,91
Incoming waves	O2/O1	0,91	0,90	0,95	0,95	0,93	0,96	0,90
	O3/O1	0,78	0,88	0,96	0,93	0,87	0,93	0,81
	O4/O1	0,64	0,96	1,00	0,94	0,85	0,92	0,76
	O5/O1	0,53	0,93	0,98	0,90	0,79	0,86	0,69

5.3.2 Model run 2: large area, orientation 45° towards direction of the incoming waves

For model run 2 the area is extended to include the morphological feature of Eagle's nest, and beyond. The orientation of the bathymetry is no longer perpendicular to the shoreline. Instead a standard south to north orientation was chosen, i.e. a rotation of 45°, towards the direction of the incoming waves. This leads to smaller input angles, with the intention to minimize this limitation of the model.

Offshore locations

The results of the model are still not satisfactory (see Figure 41). In fact, only waves at O2 have a smaller RMSE-value compared to model run 1 (see Table 4). Comparing RMSE-values between the offshore locations of the different runs might however be a little misleading. A big disadvantage of increasing the area is that the wave characteristics of the input, taken from measurements at O1, are no longer derived from a location close to the edge of the input area. The consequence being, that the exact values of the output can be considered valid only if there is no wave transformation occurring between the input and O1, 1.5 km away. The water depth is quite deep in this area, 10 m and more, but as mentioned previously, shallow water processes are still present. This is therefore not an acceptable assumption and it is of more interest to investigate if this model run can simulate the trend of continuous decrease in wave height found in the field data.

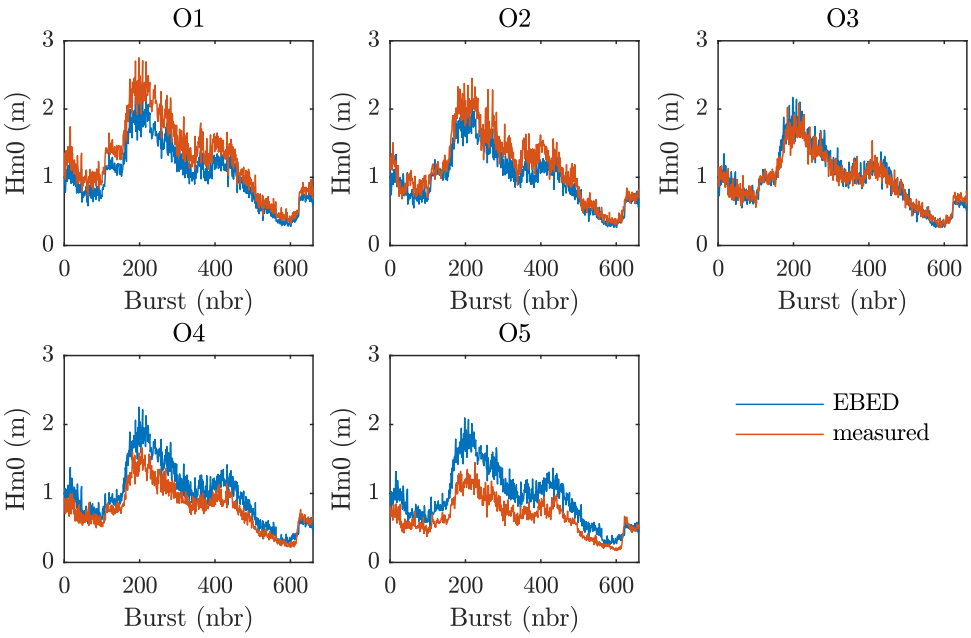

Figure 41: Result model run 2: modelled and measured values for significant wave height,H_{m0}, for all offshore location.

Figure 42 and Table 5 show that there is no real change in wave height when moving closer to shore. In addition wave height, on average, still increases between O3 and O4/O5. The model has not been successful in modelling the decrease in energy for the offshore locations.

The result of the 2D output of the model, showing direction and wave height, can be seen in Figure 43. Slightly higher wave heights occur around O1, likely due to the shallower plateau around it, as concluded earlier from the analysis of the measurements. Shoaling and refraction processes can also be detected just before and at O3-O5, leading to the large modelled wave heights found here. The sheltering effect of Eagle's nest can also clearly be seen. However, this effect reaches only the bay connected to this morphological feature and does not greatly affect the field site.

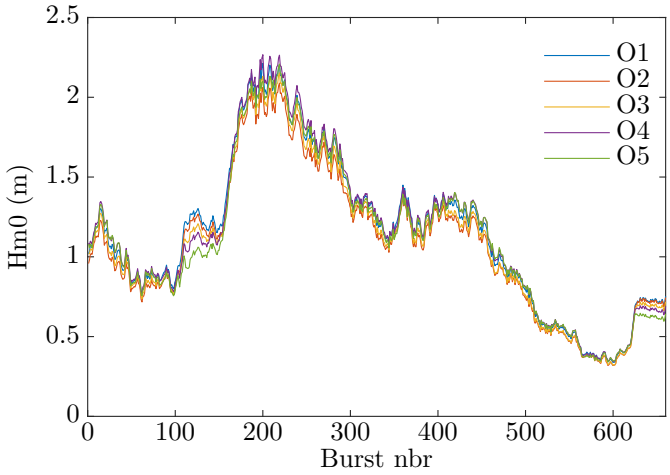

Figure 42: Result model run 2: modelled values for significant wave height, H_{m0}, for all offshore location.

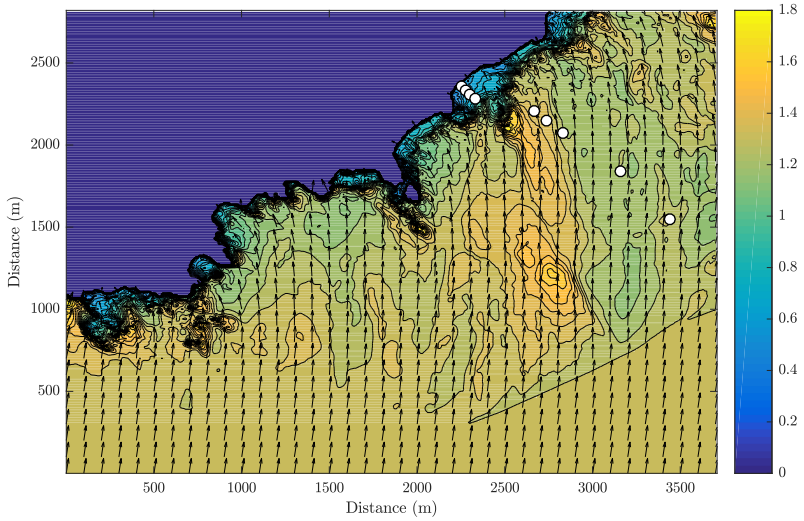

Figure 43: Result model run 2: Offshore wave transformation for burst 444, shown with wave direction (arrows) and H_{m0} (contours, scale to the right).

When comparing the direction of the input waves with the direction of the waves on the first row of the model output, a discrepancy is still present (see Figure 44). This means that the same conclusion as for model run 1 is applicable here; the modelled waves do not take the same path as the actual waves, which can lead to errors.

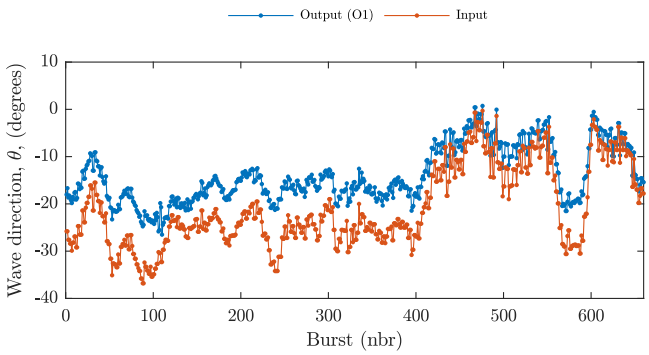

Figure 44: Result model run 2: Modelled wave direction, θ, on the first row (at O1), compared to input values.

To summarize, it can be said that a larger area and smaller values for the wave angles does not improve the model results. It is difficult to compare the actual values produced by the different model runs. This due to that the input values used are collected at a location approximately 1.5 km northwest of the input location. Instead the general trend should be evaluated. No clear improvement could be detected. The significant wave height is still very similar at all sites, compared to the measured continuous decrease when moving towards the shore. It can be concluded that this model run is not able to accurately simulate all wave transformation processes present at the site. As refraction and diffraction are the prominent processes responsible for decrease in wave height, it is likely that this model setup has not been able to represent the right effect of these processes.

Platform locations

Due to the fact that the waves on the platform are mainly controlled by water depth and not as largely affected by offshore wave conditions it is more acceptable to compare absolute values for these locations. The model output for waves on the platform follows the same trend as for the previous run with very similar wave heights, they have however decreased slightly, resulting in smaller errors (see Table 4). This is possibly due to the fact that the real path of the waves is

better represented by the larger area and smaller values for the directional angles or could be due to change in wave height for waves reaching the platform.

5.3.3 Model run 3: large area, orientation 45° towards direction of the incoming waves, extra angle

The analysis of the previous results has suggested that the model is not able to, in a satisfactory way, simulate the effect of refraction and diffraction for this complex situation. It has been proven that the model's directional output at row 1 is continuously lower than the input values (see Figure 38 and 44). This could lead to that the effect of the shallow areas south west of the field site, which are believed to be the reason for the change in wave height between O3, O4 and O5, are not taken into account correctly. To investigate if a larger angle on the first row of the output could lead to a simulation which represents the measured decrease in wave height, the model is run with an increased angle. The incoming wave direction is therefore increased by 25°.

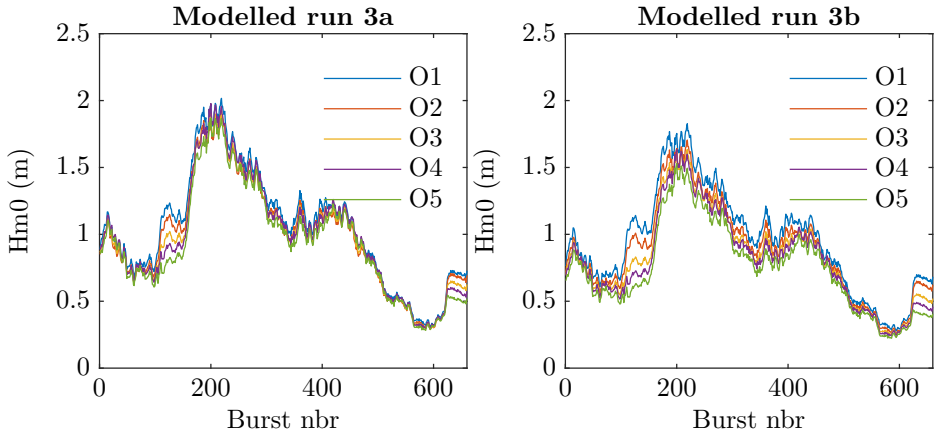

(a) Model run 3a

(b) Model run 3b

Figure 45: Result model run 3a and 3b: modeled values for significant wave height,H_{m0}, for all offshore location.

Offshore locations

The same reasoning as for run 2 stands here; the absolute values are not confidently comparable due to the origin of the input values. Instead a general trend should be analysed. The significant wave height is still very similar between sites and the rather large continuous decrease shown in the measurements has not

been accurately simulated (see Figure 45a). It should though be noted that the wave height is, for the first time, showing a trend of decrease when moving closer to shore (see Table 5). An exception is the change between O3 and O4, where on average, no significant change was detected. For the earlier model runs, the largest increase in wave height was detected between these two sites, leading to the conclusion than an improvement has in fact occurred.

To investigate this even further the angle is increased by an additional 20°, this to explore if larger proportional decrease between sites can be simulated. The result shows a clear decrease between sites, but the proportional decrease is still not as large as the measured one (see Figure 45b and Table 5.

Figure 46 shows the directions of the input and output waves at O1. The output direction for 3.a is rather close to the measured direction, whereas the incoming angle is larger, with values around 30-50°, for run 3.b. In this case, all waves are propagating close to parallel to shore; the limit of realistic angles has been reached, even when looking at the output of the model.

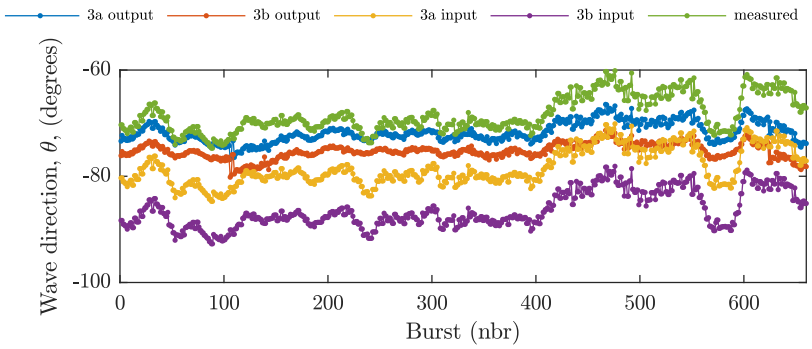

Figure 46: Result model run 3: Modelled wave direction, θ, on the first row (at O1), compared to input values for both model run 3a and 3b.

Figure 47 and 48 show the output for the whole domain for the runs with increased angle of propagation. The pattern in wave height for the two runs is very similar, although run 3.b. is presenting lower waves. The extent of the shadowing effect of Eagle's nest has increased compared to run 2 and is similar for both cases within run 3. A smaller increase of wave heights over the platform ridge can be seen for 3.b. This is likely the reason for the better fit with the measured data.

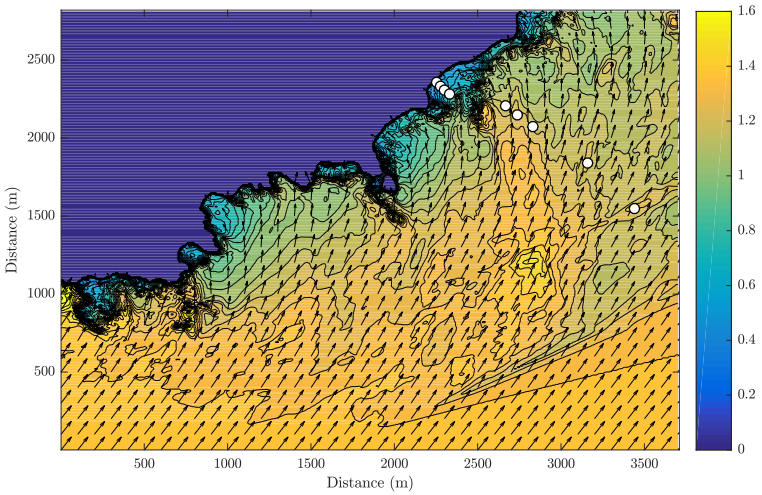

Figure 47: Result model run 3a: Offshore wave transformation for burst 444, shown with wave direction (arrows) and H_{m0} (contours, scale to the right).

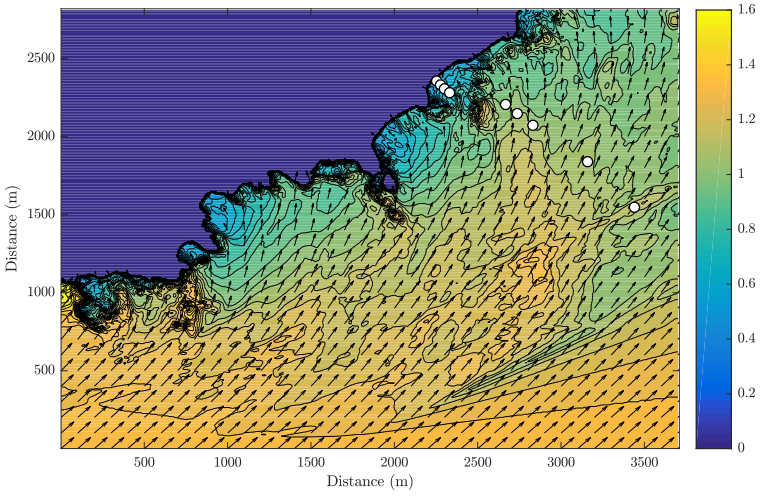

Figure 48: Result model run 3b: Offshore wave transformation for burst 444, shown with wave direction (arrows) and H_{m0} (contours, scale to the right).

Platform locations
The result of the simulation for the platform locations is similar to the previous results with some improvement for all sites (see Table 4). Especially for 3.b the agreement is better for P1 and P2 and the model is not overpredicting as much. This is likely due to the smaller wave heights which are produced by this run, showing that not only the stable wave height, or breaking index, but also the offshore wave conditions are controlling factors for waves on the platform. The fact that the measured wave heights on the platform are lower for the second high tide peak, where incipient waves are smaller, strengthens this theory.

5.3.4 Model run 4: Spectral Analysis

The EBED model is based on spectral wave transformation and uses the input wave characteristics to produce a JONSWAP spectrum with standard parameters. The spectrum produced by the model is compared to the field data (see Figure 49). Figure 49a shows the result for one burst for model run 1 at O1, but the same trend can be seen in the remaining data and for all bursts, sites and runs: the spectra used by the model show much higher and narrower peaks than the measurements.

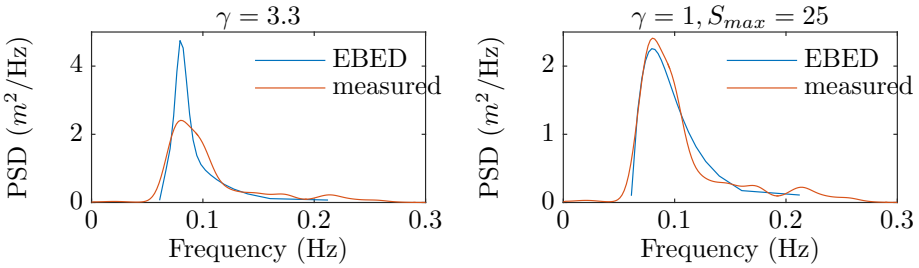

(a) Wave spectra with $\gamma = 3.3$

(b) Wave spectra with $\gamma = 1$

Figure 49: JONSWAP spectrum produced by EBED model at burst 444 for model run 1, compared to field data.

The shape of the JONSWAP spectrum can be adjusted by changing its parameters, one being the peakedness parameter γ which determines the concentration of the spectrum at the peak frequency. Instead of using a standard value of 3.3, γ can be estimated, using T_p and H_{m0}, by a relationship based on qualitative considerations of deep water wave data from the North Sea developed by Torsethaugen et al. [1985] (see Equation 21).

$$D = 0.036 - 0.0056 * T_p/\sqrt{(H_{m0})} \tag{21a}$$

$$\gamma = exp(3.484 * (1 - 0.1975 * D * T_p^4/(H_{m0}^2))); \tag{21b}$$

For the present field data, this estimation gives a peakedness factor of 1 or below for all bursts. This means that the measured waves are long compared to their height, relative to the standard sea. When using $\gamma = 1$ the fit of the simulated spectrum is notably increased (see Figure 49b).

Model run 3.a and 3.b has presented the best model performance, the same conditions have therefore been used to investigate the potential improvement when adjusting the spectrum parameters. Figure 50 shows the result of the model simulations with the adjusted value for γ.

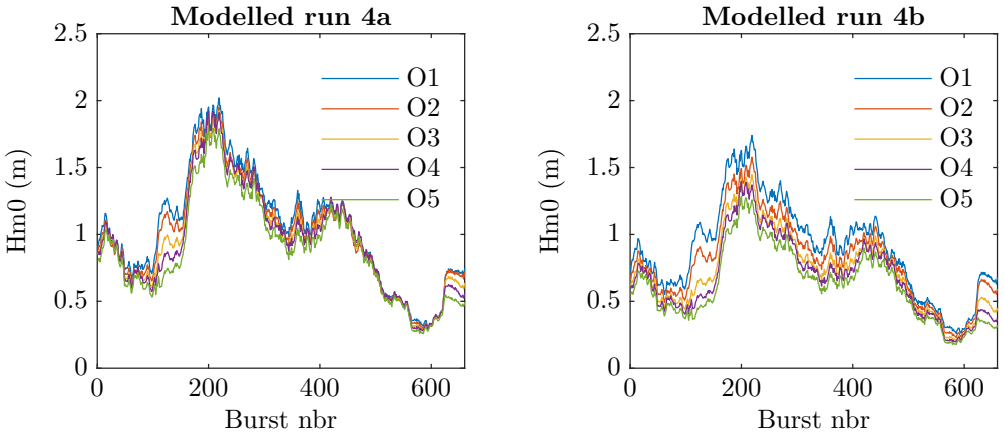

(a) Model run 4.a.

(b) Model run 4.b.

Figure 50: Result model run 4: modelled values for significant wave height H_{m0}, for all offshore locations.

Offshore locations

The result for model run 4.a shows an improvement compared to run 3.a (see Figure 50a and Table 5). The significant wave height decreases between all sites. In particular, between O4 and O5, there is now a detectable average decrease in wave height. It should though be said that the changes in average wave height between sites are still small (between 96-86 % of incoming wave height).

The decrease of wave height between sites is the largest for model run 4.b (see Figure 50b and Table 4). This run corresponds best to the measured wave characteristics but is still not in complete agreement. The proportional decrease in wave height is very similar to the field data for O2 and O3. The modelled

change between O3, O4 and O5 is though not quite sufficient, still, the agreement is rather good and significantly better than for any other model run.

For this best model run the variability of the waves reaching the studied platform and some of the surrounding platforms was analysed. Figure 51 and 52 shows the model output for the area around the platform edge for a low tide and high tide situation respectively. A large variability in wave heights can be seen both for different platforms and along the same platform for both tidal states. It is clear that, in general, the western parts of the platforms are protected from larger waves due to the direction of the waves. Larger waves can instead generally be found at the eastern sides. This trend is though not as clear on at the field site, where conditions seam more chaotic. This can be explained by a relatively small headland present at the western end of the platform, compared to other platforms, offering less protection, in combination with the shallow ridge causing a more complex wave transformation off the edge of the platform.

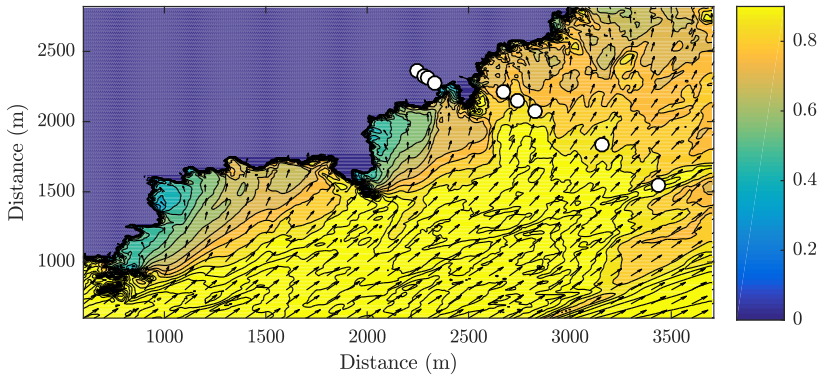

Figure 51: Result model run 4b: Low tide wave conditions and wave transformation around the platform for burst 424, shown with wave direction (arrows) and H_{m0} (contours, scale to the right).

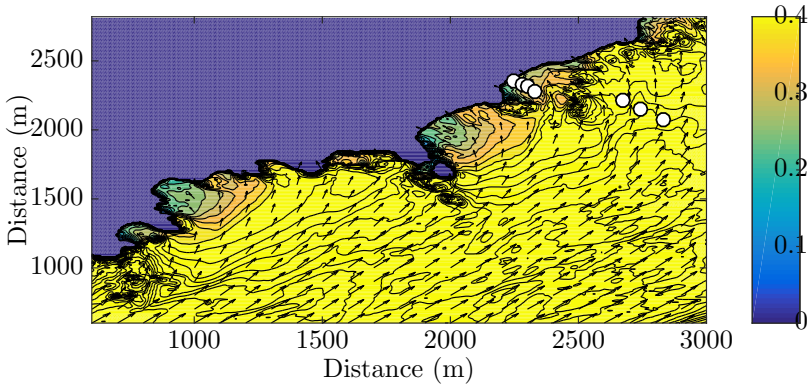

Figure 52: Result model run 4b: High tide wave conditions and wave transformation around the platform for burst 424, shown with wave direction (arrows) and H_{m0} (contours, scale to the right).

Platform locations

The predictions of the model for run 4.a-b for the locations on the rock platform also show an increased agreement compared to run 3.a and 3.b respectively. The result from run 4.b shows the best model fit also for the platform locations with the lowest RMSE-values for all sites (see Table 4). The same explanation as presented for run 3 is valid here. The smaller predicted wave heights for the waves off the platform are likely the reason for the smaller wave heights on the platform. It can be seen that model run 4.b. presents the best agreement, i.e. lowest RMSE-value, for the most shoreward offshore location O5, meaning that the predicted waves just off the platform are more similar to the waves measured in the field. This is likely the reason for the better predictions on the platform.

6 Discussion

The most important finding from the collected measurements is the large decrease in wave height for the offshore locations. A trend which could not be reproduced by the modified EBED model. This means that there are processes present which are not included or accurately represented by the model. The chosen field site shows rather unique and complex conditions for wave transformation. The extremely large angles in combination with the complicated bathymetry in the nearby surroundings and the waves' deviation from the standard shape of the wave spectrum creates a difficult situation for wave modelling. The decrease in wave height is most likely due to diffraction and refraction processes connected to shallow areas located further west on the coast. The modified EBED model has not been able to simulate these transformation processes. This even though the model is designed for and has previously been successful in the modelling of diffraction and refraction processes. Several different factors could have contributed to the modified EBED model's poor performance on the field site.

Firstly the issue with the large incoming angles and the model's limitation in accurately reproducing waves with similar directions, even on the first row of the output, will be discussed. The model uses the wave characteristics, H_{m0}, T_s and $\overline{\theta}$, to produce a wave spectrum which is used for the energy balance equation. When the offshore wave spectrum is calculated, the spectrum density is divided into a number of frequency and direction bins. During the modelling the spectrum density is then integrated over all these bins in order to obtain the direction based on this density. If the offshore wave angle is small the wave direction on the first row is quite similar to the input value. However, if the input value of the wave angle is large, or very large, then the mean wave angle on the first row could be significantly smaller, which is likely to be mainly due to the integration when obtaining the spectrum density.

In order to investigate if this limitation in the model is the reason for the poor agreement with the measured values, the extreme case scenarios (model run 3b and 4b) were performed. In fact for run 4b the model output is acceptable, and a large decrease in wave height has been detected. These extreme case scenarios contain some large limitations. Firstly, as previously mentioned, the location of the input offshore waves are an issue. For more reliable results wave characteristics should have instead been measured at a location closer to the edge of the model area. An alternative could have been to estimate the wave transformation backwards between O1 and the edge of the model area in order to estimate the wave characteristics at the wanted location. Due to time limitations, this was unfortunately not done. Another limitation of the best fit model run is the extent of the available bathymetry data. An approximate value of 23 m is set for unavailable offshore water depths. As mentioned previously, even the shortest

period waves start interacting with the bottom at a depth of 19 m, a depth limit which is much larger for longer period waves. Some wave transformation processes could hence have been missed in these areas and further offshore. Following this, it can be concluded that the first row of the model area can not be considered as being in true deep water conditions. As a consequence it is uncertain if the wave characteristics can be assumed to be constant for the whole input row of the model. This could have been avoided if more bathymetry data was available in order to extend the model area further off shore.

Another related source of error could be the directional data obtained from the Port of Melbourne wave rider buoy positioned at Point Nepean. Point Nepean is located approximately 80 km west of the field site and even though it is acceptable to assume that the deep water wave conditions are similar for the two sites, a more accurate result could have been achieved with more locally obtained data. Especially due to the previously drawn conclusion of the presence of near shore processes already at the first row, indicating that the offshore wave direction could have changed before reaching the model area. In addition there are some uncertainties regarding the measurements and the conversion of these into wave parameters. Firstly the probes were not calibrated before deployment which could have lead to potential errors. Secondly the conversion from pressure to water level is based on a constant, average estimation of barometric pressure. This can lead to errors if there are large fluctuations in barometric pressure during the measurement period. To avoid this an air pressure sensor could have been installed.

The grid size of the bathymetry matrix is another factor which could have affected the performance of the model. A smaller grid size could have more accurately represented the features of the bottom and hence lead to a better agreement. This is particularly true for the sites on the platform where the bottom surface is irregular and water levels are small.

To enable more confident conclusions about wave transformation processes, the transect of measurement locations could have been more in line with the direction of the waves. In such a case, the path of the waves could have been followed and the change of wave characteristics during the wave's propagation towards shore could have been analysed.

Even though the model simulations have not been quite successful for the studied site they still illustrate the fact that wave transformation processes are present. The results clearly show how important offshore bathymetry is in controlling the characteristics of waves reaching rock platforms. This can partly be concluded from the difficulty in accurately simulating the wave transformation processes at the field site but can also be discussed by looking at the 2D output from the wave model (see Figure 47, 48, 51 and 52). All bays in the close proximity of the field site are lined with rock platforms. The nearshore wave

transformations in the different bays do not follow the same pattern. The two bays to the west of the field site show a simpler morphology and bathymetry and a more gradual decrease in wave height within the bay (see Figure 13). Some consequences of the extreme wave directions can be seen also here. Larger waves reach the eastern sides of the platforms whereas the western sides are largely sheltered by the headlands surrounding the bays. When comparing bays in this way, it is once again clear how complex the conditions at the field site are. The pattern in wave height and wave direction in the studied bay does not follow such a gradual decrease and appears more chaotic.

When moving onto the platform the model output is in better agreement with the measurements. The model, as well as the field data, shows a large control of water depth on platform waves. In addition a small effect of offshore wave height can be seen in the model output, with larger wave heights for stormier conditions, a trend previously seen in the research. The same tendency can be seen for the field measurements, although the limited amount of data does not allow any confident conclusions regarding this. The model's overprediction regarding the simulation of the offshore wave height is therefore also affecting the model prediction on the platform. A fact that can be seen in the results. The best model fit on the platform corresponds with the best fit of data to O5 (model run 4b). For this run the RMSE at O5 is as low as 0.123, which can be seen as a good agreement, and the results for the platform sites are rather good for all sites (RMSE between 0.029-0.046). Still, all model predictions show slightly higher peaks in wave height during high tide, compared to the data. This can be compared with the conclusion about the breaking index, H_{m0}/h, found in the data. The average value of $\gamma_{b_{m0}} = 0.33$ is somewhat lower than, but in the range of, what has generally been found in previous research (see Table 1). As already discussed, the underlying reason for this is likely to be due to the local morphology of the platform and as mentioned previously a smaller grid size of the bathymetry matrix could have led to a more accurate model output on these sites.

7 Conclusion

This study has shown that the modified EBED model has not been able to accurately simulate all the measured wave transformation processes offshore the studied rock platform. The chosen field site possesses rather unique and complex conditions for wave transformation. The extremely large angles in combination with the complicated bathymetry in the nearby surroundings and the waves' deviation from the standard shape of the wave spectrum creates a difficult situation for wave modelling. The model's limitation in handling input waves with large angles is concluded to be one of the main reasons for the discrepancy between simulations and field data.

The results for the locations on the platform show a better agreement although slightly lower measured wave heights have been found. This is concluded to be partly due to the overestimation of the offshore wave heights and the morphological features of the platform. The substrate is sometimes greatly uneven with bolder like features, an effect which lost in the modelling due to the relatively big grid size. The lower wave heights for the measurements corresponds with the fact that rather low breaking indexes have been concluded from the field data, compared to previous studies, indicating lower than average wave heights compared to water depth.

The two dimensional output from the wave model illustrates the importance of offshore bathymetry for wave dynamics at a rock platform. The nearshore wave transformation processes are important in controlling the characteristics of the waves reaching a rock platform and the model shows a large variation between and within a specific site.

The rather poor agreement of the model on this specific site does not mean that wave modelling on, and offshore from, rock platforms is not to be done. It is highly likely that the results of the wave simulations would have produced an acceptable result for sites with less complexity. A simpler site, with an area reaching out to true deep water wave conditions, should be used for further analysis of the applicability of the modified EBED model, or other numerical wave models, on rocky shore platforms.

References

T. Baldock. Dissipation of incident forced long waves in the surf zone—implications for the concept of "bound" wave release at short wave breaking. *Coastal Engineering*, 60:276–285, 2012.

J. Battjes, H. Bakkenes, T. Janssen, and A. Van Dongeren. Shoaling of subharmonic gravity waves. *Journal of Geophysical Research: Oceans*, 109(C2), 2004.

E. P. Beetham and P. S. Kench. Field observations of infragravity waves and their behaviour on rock shore platforms. *Earth Surface Processes and Landforms*, 36(14):1872–1888, 2011.

M. Buckley, R. Lowe, and J. Hansen. Evaluation of nearshore wave models in steep reef environments. *Ocean Dynamics*, 64(6):847–862, 2014.

C. V. P. Commonwealth of Australia-Bureau of Meteorology National Tide Centre, Port Melbounre Corporation. *Victorian Tide Tables 2013*. Port of Melbourne Corporation, 2013.

W. R. Dally, R. G. Dean, and R. A. Dalrymple. Wave height variation across beaches of arbitrary profile. *Journal of Geophysical Research*, 90(C6):11917–11927, 1985.

U. A. C. O. Engineers. Coastal engineering manual. *Engineer Manual*, 1110: 2–1100, 2002.

E. J. Farrell, H. Granja, L. Cappietti, J. T. Ellis, B. Li, and D. J. Sherman. Wave transformation across a rock platform, belinho, portugal. *Journal of Coastal Research*, pages 44–48, 2009.

Google Maps. Australia. Retrieved from: https://www.google.com.au/maps/@-25.335448,135.745076,4z, 2016.

M. Gourlay. Wave transformation on a coral reef. *Coastal Engineering*, 23(1): 17–42, 1994.

S. M. Henderson, R. Guza, S. Elgar, T. Herbers, and A. Bowen. Nonlinear generation and loss of infragravity wave energy. *Journal of Geophysical Research: Oceans*, 111(C12), 2006.

L. H. Holthuijsen. *Waves in oceanic and coastal waters*. Cambridge University Press, 2007.

T. Janssen, J. Battjes, and A. Van Dongeren. Long waves induced by short-wave groups over a sloping bottom. *Journal of Geophysical Research: Oceans*, 108 (C8), 2003.

P. Kench, R. W. Brander, K. E. Parnell, and J. O'Callaghan. Seasonal variations in wave characteristics around a coral reef island, south maalhosmadulu atoll, maldives. *Marine geology*, 262(1):116–129, 2009.

D. M. Kennedy. Where is the seaward edge? a review and definition of shore platform morphology. *Earth-Science Reviews*, 147:99–108, 2015.

D. M. Kennedy, S. Sherker, B. Brighton, A. Weir, and C. D. Woodroffe. Rocky coast hazards and public safety: moving beyond the beach in coastal risk management. *Ocean & Coastal Management*, 82:85–94, 2013.

R. J. Marshall and W. J. Stephenson. The morphodynamics of shore platforms in a micro-tidal setting: Interactions between waves and morphology. *Marine Geology*, 288(1):18–31, 2011.

H. Mase. Multi-directional random wave transformation model based on energy balance equation. *Coastal Engineering Journal*, 43(04):317–337, 2001.

G. Masselink. Group bound long waves as a source of infragravity energy in the surf zone. *Continental Shelf Research*, 15(13):1525–1547, 1995.

J. McCowan. Vii. on the solitary wave. *The London, Edinburgh, and Dublin Philosophical Magazine and Journal of Science*, 32(194):45–58, 1891.

W. Munk. Origin and generation of waves. *Proceedings 1st International Conference on Coastal Engineering*, 1(1):1–4, 1950.

P. T. Nam, M. Larson, H. Hanson, et al. A numerical model of nearshore waves, currents, and sediment transport. *Coastal Engineering*, 56(11):1084–1096, 2009.

L. Naylor, W. Stephenson, and A. Trenhaile. Rock coast geomorphology: recent advances and future research directions. *Geomorphology*, 114(1):3–11, 2010.

R. C. Nelson. Design wave heights on very mild slopes: an experimental study. *Transactions of the Institution of Engineers, Australia. Civil engineering*, 29 (3):157–161, 1987.

H. Ogawa. Observation of wave transformation on a sloping type b shore platform under wind-wave and swell conditions. *Geo-Marine Letters*, 33(1):1–11, 2013.

H. Ogawa, M. Dickson, and P. Kench. Wave transformation on a sub-horizontal shore platform, tatapouri, north island, new zealand. *Continental Shelf Research*, 31(14):1409–1419, 2011.

H. Ogawa, P. Kench, and M. Dickson. Field measurements of wave characteristics on a near-horizontal shore platform, mahia peninsula, north island, new zealand. *Geographical Research*, 50(2):179–192, 2012.

H. Ogawa, M. E. Dickson, and P. S. Kench. Hydrodynamic constraints and storm wave characteristics on a sub-horizontal shore platform. *Earth Surface Processes and Landforms*, 40(1):65–77, 2015.

T. Poate, G. Masselink, M. Austin, M. Dickson, , and P. Kench. Observation of wave transformation on macro-tidal rocky platforms. *Journal of Coastal Research*, Special Issue(No. 75):XX–XX, 2016.

A. Pomeroy, R. Lowe, G. Symonds, A. Van Dongeren, and C. Moore. The dynamics of infragravity wave transformation over a fringing reef. *Journal of Geophysical Research: Oceans*, 117(C11), 2012.

T. Shand, W. Peirson, M. Banner, and R. Cox. Predicting hazardous conditions for rock fishing—a physical model study. *Manly Vale (AUST): University of New South Wales Water Research Laboratory*, 2009.

A. Short and C. Woodroffe. *The Coast of Australia*. Cambridge University Press, 2009. ISBN 9780521873987. URL `https://books.google.se/books?id=whZcIO7zLjEC`.

J. Simm, A. Brampton, N. Beech, C. I. Research, I. Association, and J. Brooke. *Beach Management Manual*. CIRIA report. Construction Industry Research and Information Association, 1996. ISBN 9780860174387. URL `https://books.google.com.au/books?id=HiIYAQAAIAAJ`.

W. Stephenson. Shore platforms: a neglected coastal feature? *Progress in Physical Geography*, 24(3):311–327, 2000.

W. J. Stephenson and R. M. Kirk. Development of shore platforms on kaikoura peninsula, south island, new zealand: Part one: the role of waves. *Geomorphology*, 32(1):21–41, 2000.

W. J. Stephenson and L. E. Thornton. Australian rock coasts: review and prospects. *Australian Geographer*, 36(1):95–115, 2005.

G. G. Stokes. On the theory of oscillatory waves. In *Mathematical and Physical Papers vol.1*, volume 1, pages 197–229. Cambridge University Press, 2009. ISBN 9780511702242. URL

http://dx.doi.org/10.1017/CBO9780511702242.013. Cambridge Books Online.

T. Sunamura. *Geomorphology of rocky coasts*. Coastal morphology and research. J. Wiley, 1992. ISBN 9780471917755. URL https://books.google.com.au/books?id=vF7uAAAAMAAJ.

B. Thom. Geography, planning and the law: a coastal perspective. *Australian Geographer*, 35(1):3–16, 2004.

E. B. Thornton and R. T. Guza. Energy saturation and phase speeds measured on a natural beach. *Journal of Geophysical Research: Oceans*, 87(C12): 9499–9508, 1982. ISSN 2156-2202. doi: 10.1029/JC087iC12p09499. URL http://dx.doi.org/10.1029/JC087iC12p09499.

K. Torsethaugen, T. Faanes, and S. Haver. Characteristics for extreme sea states on the norwegian continental shelf. Technical report, 1985.

A. Trenhaile. *The geomorphology of rock coasts*. Oxford Research Studies in Geography Series. Oxford University Press, Incorporated, 1987. ISBN 9780198232797. URL https://books.google.com.au/books?id=plruAAAAMAAJ.

A. S. Trenhaile. Rock coasts, with particular emphasis on shore platforms. *Geomorphology*, 48(1):7–22, 2002.

A. S. Trenhaile and J. I. Kanyaya. The role of wave erosion on sloping and horizontal shore platforms in macro-and mesotidal environments. *Journal of Coastal Research*, pages 298–309, 2007.

C.-H. Tsai, M.-Y. Su, and S.-J. Huang. Observations and conditions for occurrence of dangerous coastal waves. *Ocean engineering*, 31(5):745–760, 2004.

M. J. Tucker and E. G. Pitt. *Waves in ocean engineering*. Number Volume 5. 2001.

A. Van Dongeren, R. Lowe, A. Pomeroy, D. M. Trang, D. Roelvink, G. Symonds, and R. Ranasinghe. Numerical modeling of low-frequency wave dynamics over a fringing coral reef. *Coastal Engineering*, 73:178–190, 2013.